

Nanoscale

Accepted Manuscript



This is an *Accepted Manuscript*, which has been through the Royal Society of Chemistry peer review process and has been accepted for publication.

Accepted Manuscripts are published online shortly after acceptance, before technical editing, formatting and proof reading. Using this free service, authors can make their results available to the community, in citable form, before we publish the edited article. We will replace this *Accepted Manuscript* with the edited and formatted *Advance Article* as soon as it is available.

You can find more information about *Accepted Manuscripts* in the [Information for Authors](#).

Please note that technical editing may introduce minor changes to the text and/or graphics, which may alter content. The journal's standard [Terms & Conditions](#) and the [Ethical guidelines](#) still apply. In no event shall the Royal Society of Chemistry be held responsible for any errors or omissions in this *Accepted Manuscript* or any consequences arising from the use of any information it contains.

Nanopatterned Polymer Brushes: Conformation, Fabrication and Applications

Qian Yu^{e*}, Linnea K. Ista,^d Renpeng Gu,^{bc} Stefan Zauscher,^{abc} and Gabriel P. López^{abcd*}

^a Department of Biomedical Engineering, Duke University, Durham, NC, 27708, USA.

^b Department of Mechanical Engineering and Materials Science, Duke University, Durham, NC, 27708, USA.

^c NSF Research Triangle Materials Research Science & Engineering Center, Duke University, Durham, NC, 27708, USA.

^d Center for Biomedical Engineering and Department of Chemical and Biological Engineering, The University of New Mexico, Albuquerque, NM, 87131, USA.

^e College of Chemistry, Chemical Engineering and Materials Science, Soochow University, Suzhou, 215123, China.

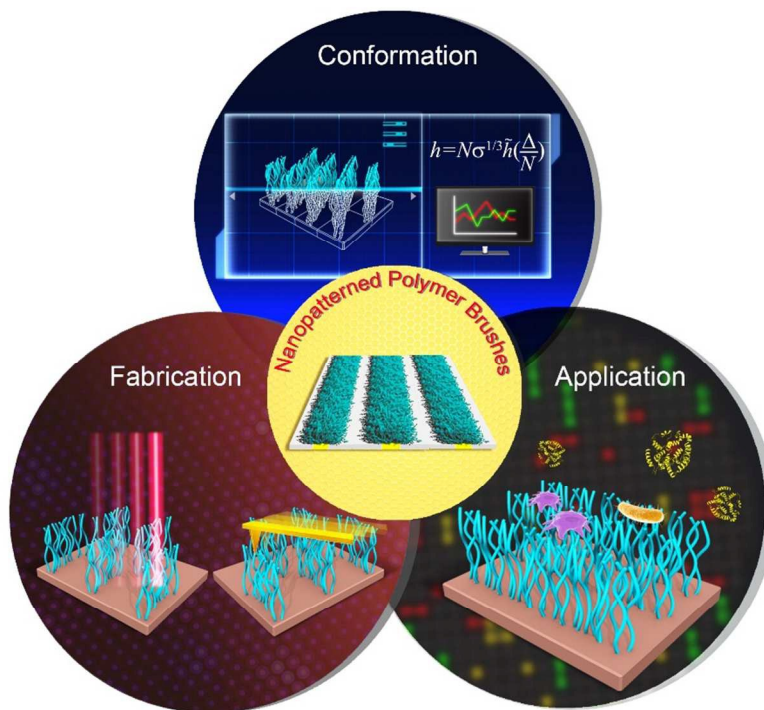
* gabriel.lopez@duke.edu; yuqian@suda.edu.cn

Abstract

Surfaces with end-grafted, nanopatterned polymer brushes that exhibit well-defined feature dimensions and controlled chemical and physical properties provide versatile platforms not only for investigation of nanoscale phenomena at biointerfaces, but also for the development of advanced devices relevant to biotechnology and electronics applications. In this review, we first give a brief introduction of scaling behavior of nanopatterned polymer brushes and then summarize recent progress in fabrication and application of nanopatterned polymer brushes. Specifically, we highlight applications of nanopatterned stimuli-responsive polymer brushes in the areas of biomedicine and biotechnology.

Keywords: nanopatterned polymer brushes; surface initiated polymerization; nanolithography

TOC



1 Introduction

Polymer brushes --ensembles of densely packed polymer chains that are tethered with one end to a surface-- are versatile materials for tailoring surface functionality and morphology.¹⁻³ Patterned polymer brushes with controllable, spatially distributed chemical and physical properties are increasingly used in fundamental research and are proposed for a variety of practical applications. The convergence of burgeoning developments in both nanofabrication techniques and synthetic methods for forming polymer brushes has driven research focused on creation and study of nanopatterned polymer brushes (NPBs), in which surface tethered polymers that have molecular size (*i.e.* contour lengths) that are comparable to the areas over which they are patterned.^{4,5} These versatile platforms enable the study of unique nanoscale phenomena, and have spurred the development of advanced materials and devices for biotechnology and electronics applications.⁴⁻⁷ Our groups have been especially engaged in proof-of-principle studies that indicate that NPBs have great potential as engineered biointerfaces, for example, in applications ranging from biosensing, to cell culture, to antifouling surfaces.⁸

NPBs exhibit unique morphological and functional properties. For example, polymer chains end-tethered on nanoscale footprints can lack lateral restraint and thus adopt a less extended conformation compared with homogeneously-grafted brushes.⁹ Moreover, the height of NPBs scales with the grafting density and with the pattern size; *i.e.*, the polymer brush height decreases with decreasing extent of the pattern footprint.^{10,11} Combined with periodicities on the length scale of the polymer molecules themselves, this effect can lead to interactions between polymer chains on adjacent parts of a nanopattern, and can provide additional functionality that is unavailable to micropatterned brushes.¹²⁻¹⁴ For example, we observed that, when NPBs are well solvated, the chains from adjacent nanopatterned

areas can overlap above the ungrafted areas of the nanopattern to interact physically.⁸ Upon an environmentally-induced transition to a poorly solvated state, however, this overlap and interaction is diminished and ungrafted portions of the substrate can be exposed. Such NPB behavior can be used to effectively and precisely control the access of solutes to the ungrafted substrate areas between adjacent, nanopatterned brushes. That is, extended, solvated brushes can provide a diffusive barrier to transport of solutes, and thus change the rate and extent of adsorption/desorption of a variety of components (*e.g.*, physically or chemically adsorbing macromolecules and nanoparticles) to/from the substrate surface.

Polymer brushes can be either “grafted to” nanopatterned substrates by reaction between end-functionalized polymer chains with surface-bound activated sites, or “grafted from” substrates using surface-initiated polymerization (SIP).^{1, 2} The former approach is straightforward but suffers from certain limitations including the tendency toward low grafting density and reduced film thickness.¹⁵ In contrast, controlled SIP techniques allow precise control over the grafting density, thickness, and composition of polymer brushes, making them well-suited for facile fabrication of well-defined NPBs.¹⁶⁻¹⁸

The last decade has witnessed dramatic progress in methods for nanopatterning substrates using mechanical, optical, electrical, and/or thermal means.^{4, 5} These strategies can be divided into two approaches, according to the process by which the polymer brush is patterned: (i) ***direct patterning***, in which the polymer is directly written on the substrate or the preformed homogenous polymer films are selectively removed or degraded by locally confined mechanical force or irradiation (“top-down”), and (ii) ***indirect patterning***, in which the nanopatterns of surface-bound initiators are pre-fabricated and serve as templates to graft polymer brushes *via* SIP (“bottom-up”). In the second strategy, the patterns of

initiators can be (i) generated *in situ* by UV or X-ray irradiation of a substrate; (ii) directly “written” on nanoscopic regions of the substrate; (iii) removed or degraded selectively from preformed, uniformly distributed surface-immobilized initiators; (iv) immobilized onto previously nanopatterned surfaces using selective chemistry or (v) immobilized onto nano-textured substrates.

Advances in fabrication techniques have enabled the study of NPBs for a range of applications. For example, nanopatterned stimuli-responsive polymer brushes are able to dynamically control surface wettability;^{19,20} NPBs incorporated on microchips and biosensors allow for the absorption of proteins and other functional biomolecules from very small volumes and, thus, enable miniaturized, multiplexed diagnostics.^{21,22} In addition, because cells are known to respond to nanometer-scale surface chemical and topographical cues, NPBs with controllable size, functionality, and physico-chemical properties provide excellent experimental platforms to study cell-surface interactions.^{23,24} We recently reported a system with switchable bioactivity based on nanopatterned stimuli-responsive polymer brushes that exploits triggered molecular conformational changes to control surface bio-recognition and cellular adhesion at the nanoscale.^{8,25-28} Moreover, after modification with stimuli-responsive polymer brushes, nanoporous substrates such as mesoporous silica,²⁹ porous silicon (pSi),³⁰ silicon nanowire arrays (SiNWAs),³¹ and anodic aluminum oxide (AAO)^{32,33} can serve as reservoirs for on demand- triggered release of drugs, proteins or other molecules.

This *review* provides a survey of recent advances made in the theory, simulation, fabrication, and application of NPBs. The first part summarizes studies of NPB scaling behavior, and presents strategies that are used for the fabrication of NPBs including direct patterning of polymer brushes, and the combination of nanolithography and surface initiated polymerization. The second part highlights

applications of NPBs including their use (i) to control surface wettability, (ii) as templates to pattern biomolecules, (iii) as platforms to investigate cell-substrate interactions, (iv) as actuators to control surface bioactivity, and (v) as stimuli-responsive “gates” to control release of molecules from nanoporous materials.

2 Scaling Relationships for NPBs

The implementation of patterned polymer brushes in micro and nanotechnology applications requires precise control of pattern shape, feature dimension, grafting density and pattern spacing, and thus, an understanding of nanopatterned brush physics. As with unpatterned brushes, the conformational behavior of surface tethered polymers is highly dependent on interactions between polymer chains, between polymer and solvent and between polymer and the substrate.^{34, 35} In addition, nanopatterned brushes are significantly affected by the size of the grafting footprint and by the chemistry of the surrounding, non-grafted surface area. The effect of pattern size on brush conformation was first noticed by Ahn *et al.*, who prepared surface-confined poly(*N*-isopropylacrylamide) (PNIPAAm) polymer brush patterns by combining lift-off electron beam lithography (EBL) and surface-initiated atom transfer radical polymerization (SI-ATRP), using a thiol-based surface-tethered initiator (**Figure 1**).³⁶ They found that the thickness of a polymer brush grown on sub-micrometer patterns (600 nm pattern size) is significantly less (*e.g.*, 170 nm) than the thickness (*e.g.*, 300 nm) of brushes grown on micrometer-scale patterns (1.8 μm pattern size).

In general, polymer brush conformation results from an energy balance between polymer brush chain segment interactions (which are typically repulsive in good solvents) and the elastic free energy that arises from the entropic penalty associated with chain stretching. Less chain crowding occurs at the

pattern periphery and results in decreased chain stretching. On patterns with a small footprint, a larger portion of the polymer brush is affected by this edge effect. This argument thus qualitatively explains the observed decrease in polymer brush thickness with decreasing pattern footprint size for polymer brushes of equal degree of polymerization.

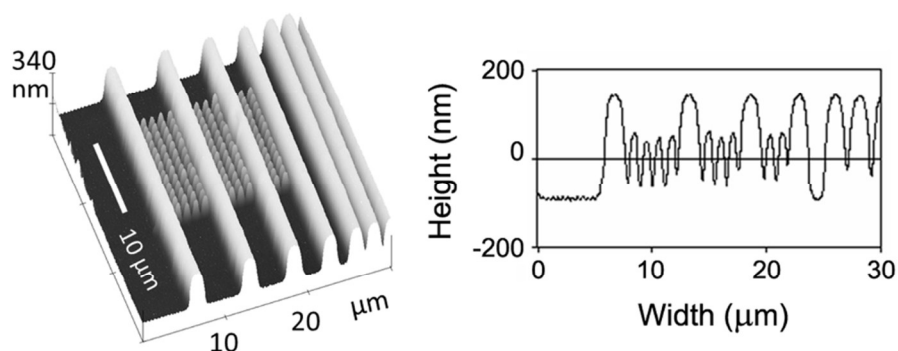


Figure 1. Tapping mode atomic force microscopy (AFM) height image (left) obtained at room temperature in air and corresponding average height profile (right) of PNIPAAm brush line micropatterns (1.8 μm wide, 300 nm high) and sub-micron patterns (600 nm wide, 170 nm high), fabricated using lift-off EBL and SI-ATRP after 90 min polymerization time. [Reprinted from Ref.³⁶ with permission, Copyright 2004, Wiley-VCH.]

To gain a more quantitative understanding of the relationship between pattern size and polymer brush conformation, Patra *et al.* simulated the static equilibrium conformation of polymer brushes as a function of pattern width using a coarse-grained model (**Figure 2**).¹⁰ In this model, the brush height, h , depends on polymer contour length, N , grafting density, σ , and pattern width, Δ . The universal scaling among these parameters is evident upon normalization of the pattern width and the grafting density by the polymer contour length, *i.e.*, Δ/N and $h\sigma^{-1/3}/N$ (**Figure 3a**). The dependencies can then be described as $h(\Delta, N, \sigma) = N\sigma^{1/3} \tilde{h}(\Delta/N)$, where $\tilde{h}(\Delta/N)$ is a universal function that ranges between 0 (for Δ/N

= 0) and a finite value (for $\Delta/N \rightarrow \infty$).

These simulations show that, with increasing Δ , the polymer brush height increases and the region of high polymer brush density expands. Specifically, when the width increases from 0.1 to 4 times the polymer contour length, the polymer brush height increases from 0.5 to full height of the homogeneously grafted brush. Furthermore, the simulations reveal that when the polymer brush regions exceed the pattern footprint width, the best scaling relationship between the excess width, w , and N , σ , and Δ , is $w(\Delta, N, \sigma) = N\sigma^{\frac{1}{2}} \tilde{w}(\Delta/N)$. Thus as σ increases, the excess width increases faster than the brush height.

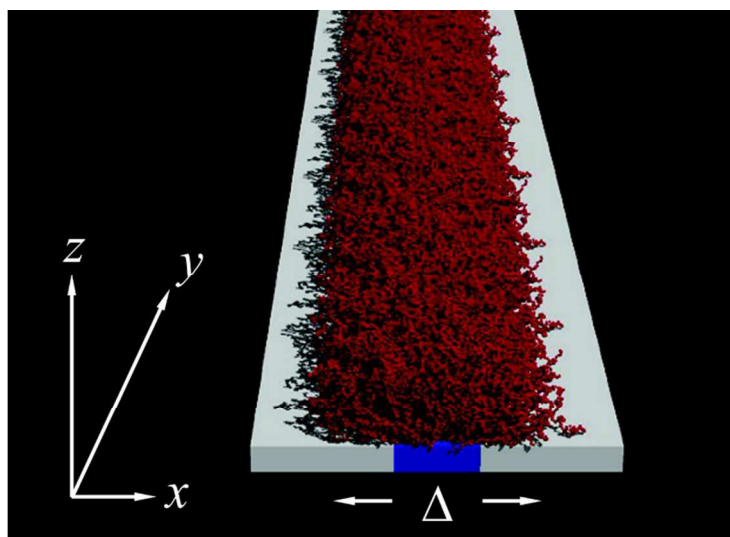


Figure 2. Snapshot illustrating the model system composed of a planar surface on which polymers are grafted onto a stripe with width, Δ . [Reprinted from Ref.¹⁰ with permission, Copyright 2006, American Chemical Society.]

To verify the simulation results, Lee *et al.* synthesized PNIPAAm brushes on pattern footprints with different sizes, and compared the measured brush heights with the scaling predictions from the coarse-grained simulations.¹¹ To do so required three assumptions: i) $h = C_1 h_{exp}$, ii) $N = C_2 h^*$, and iii) $\sigma =$

$C_3\chi_{surf}$, where h is the brush height on an unpatterned substrate, χ_{surf} is the initiator mole fraction on the surface, and C_1 , C_2 , and C_3 are constants. With these assumptions, the universal scaling relationship becomes $h_{exp}(\Delta, h^*, \chi_{surf}) = h^* \chi_{surf}^{1/3} \tilde{h}(\Delta / h_{exp})$. A comparison of **Figures 3a** and **3b** shows that the normalized experimental results generally reflect the scaling predictions from simulations.

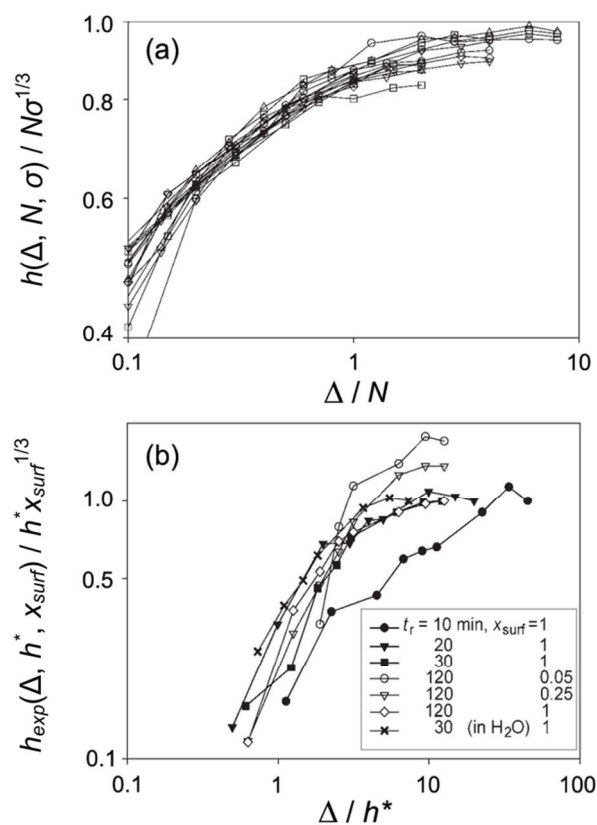


Figure 3. Scaled brush height as a function of scaled footprint size. (a) Results from a coarse-grained model¹⁰ and (b) experimental data from AFM measurements. [Reprinted from Ref.¹¹ with permission, Copyright 2007, Wiley-VCH.]

In another study, Jonas *et al.* studied the shape of poly(2-(2-methoxyethoxy)ethyl methacrylate) (PMEO₂MA) nanopatterns experimentally and described the dry shape of the polymer brush using a simple model involving chain entropy and wetting energy.¹³ This model reveals a universal relationship

between the polymer brush dry height and its lateral dimensions on nanopatterns, as shown in **Figure 4** by the dashed line, and data for PMEO₂MA, PNIPAAm, and polystyrene (PS) brushes. Here, the scaled brush height $\bar{2R}_0$ is defined as $2R_0/h_0$, where h_0 is the corresponding brush height on a surface with infinite lateral extent, and $2R_0$ is the grafting diameter. When $\bar{2R}_0 > 3$, the wetting energy can be safely ignored. However, once $\bar{2R}_0$ decreases, the wetting interaction between substrate and polymer brush becomes important. Because the polymer is surface-tethered, the entropic chain stretching energy penalty limits chain spreading on the substrate. Thus, as shown by the solid line in **Figure 4**, the nanopatterned polymer brushes behave as nanodroplets, whose shape is controlled by both chain stretching and wetting.

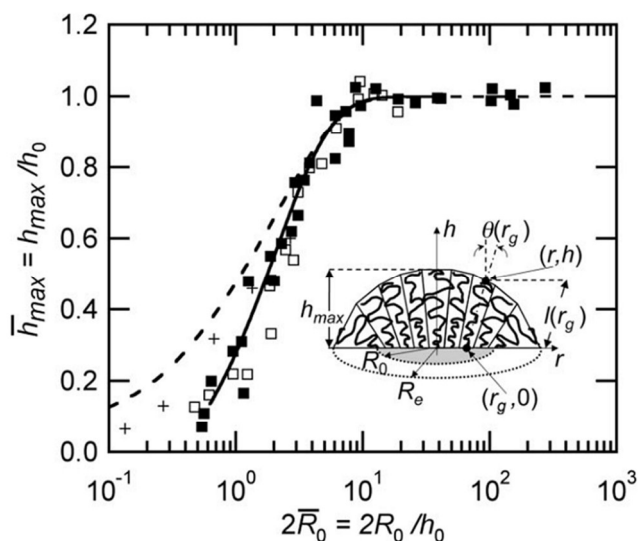


Figure 4. Normalized maximal height of nanobrushes plotted as a function of normalized grafting diameter: (▪) PMEO₂MA brushes; (◻) PNIPAAm brushes¹¹; (+) PS brushes³⁷. Dashed line: theoretical master curve incorporating chain entropy only. Continuous line: theoretical prediction incorporating chain entropy and wetting energy. The inset schematically shows a brush nanodroplet. [Reprinted from Ref.¹³ with permission, Copyright 2008, American Chemical Society.]

Alexandros *et al.* used a lattice bond fluctuation Monte Carlo method to simulate polymer brush conformation on periodically patterned stripes of different widths;¹² interactions between neighboring polymer brush stripes were considered as well. These simulations predict that for $\zeta < 0.7$ ($\zeta = \Delta/N\sigma^{1/3}$), the polymer brush morphology is similar to that of a homogeneously grafted brush with grafting density. For $\zeta > 4$, the brush forms isolated polymer stripes, and for $0.7 < \zeta < 4$, the polymer brush forms parallel pores on non-grafted areas, and exhibits a groove morphology on the brush surface. The depth of the grooves scales with ζ (Figure 5).

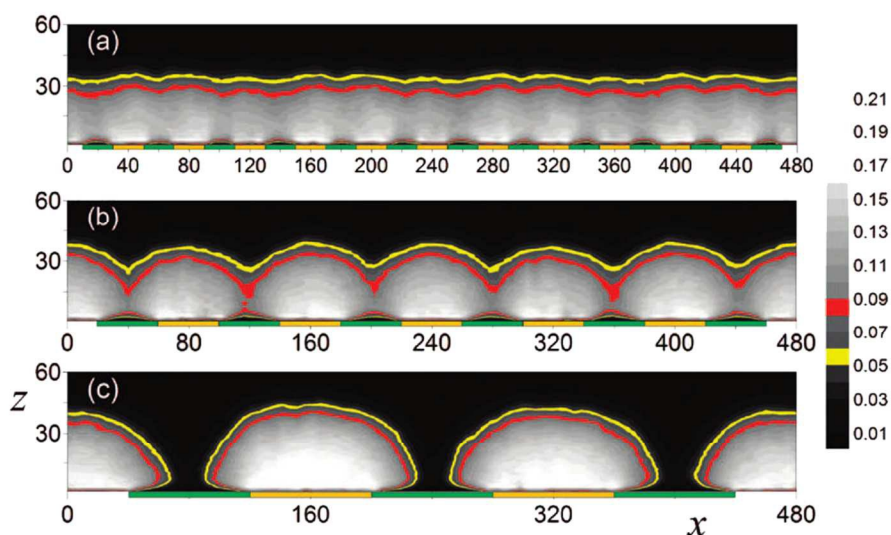


Figure 5. Representative contour plots of the average two-dimensional density profile $\phi(x,z)$ for the system with $N = 40$ and $\sigma_s = 0.1$ for various stripe widths: (a) $\Delta = 40$ ($\zeta = 1.08$), (b) $\Delta = 40$ ($\zeta = 2.15$), and (c) $\Delta = 80$ ($\zeta = 4.31$). The yellow and red contours correspond to $\phi_0 = 0.05$ and 0.08 , respectively. The alternating green and orange bars on the x -axis represent the non-grafted and grafted stripes, respectively. [Reprinted from Ref.¹² with permission, Copyright 2008, American Chemical Society.]

The pioneering simulation work of Alexandros *et al.*, provided a basis by which to interpret our

more recent experimental results on similarly patterned, stimuli-responsive brushes and provided the theoretical underpinning for the development of a number of multi-functional, nanopatterned brush systems for biomaterial applications (*vide infra*).^{8, 25-28} We fabricated a series of nanopatterned PNIPAAm brushes with varying stripe width (Δ).⁸ AFM section analysis of these brushes suggested that the nanopatterned polymer structures can be grouped into three distinct categories, corresponding to large, medium, and small Δ (**Figure 6a**). At both 25°C and 37°C (*i.e.*, above and below the lower critical solution temperature (LCST) of PNIPAAm in water), the samples with larger Δ exhibited a relatively smooth morphology of the brush surface and limited access of the AFM tip to the substrate. Conversely, the samples with smaller Δ exhibited a groove- and ridge-like topography, in which the AFM tip can come into direct contact with the substrate surface. Interestingly, for the sample with medium Δ , the variation in the peak-to-valley dimension (PVD) values of the nanopatterned PNIPAAm brushes in an aqueous environment between 25°C and 37°C is largest (**Figure 6b**). At 25°C (below the LCST of PNIPAAm), chains hydrate and adopt an extended conformation in which they spread and interact laterally to form a continuous layer that occludes the underlying patterned substrate to yield a relatively smooth surface (PVD \approx 1.6 nm). However, at 37°C (above the LCST), the pattern appears and shows a dramatic increase in the PVD value (\approx 38.0 nm) that likely corresponds to the distance between the substrate and the top of the collapsed polymer stripes. This temperature triggered topological change was switchable and repeatable for several cycles, thus enabling the spatially regulated concealment and exposure of molecules that are immobilized between the lines of nanopatterned brushes. This behavior has been exploited to control the bioactivity of surfaces, as described in more detail in **Section 4.3**.

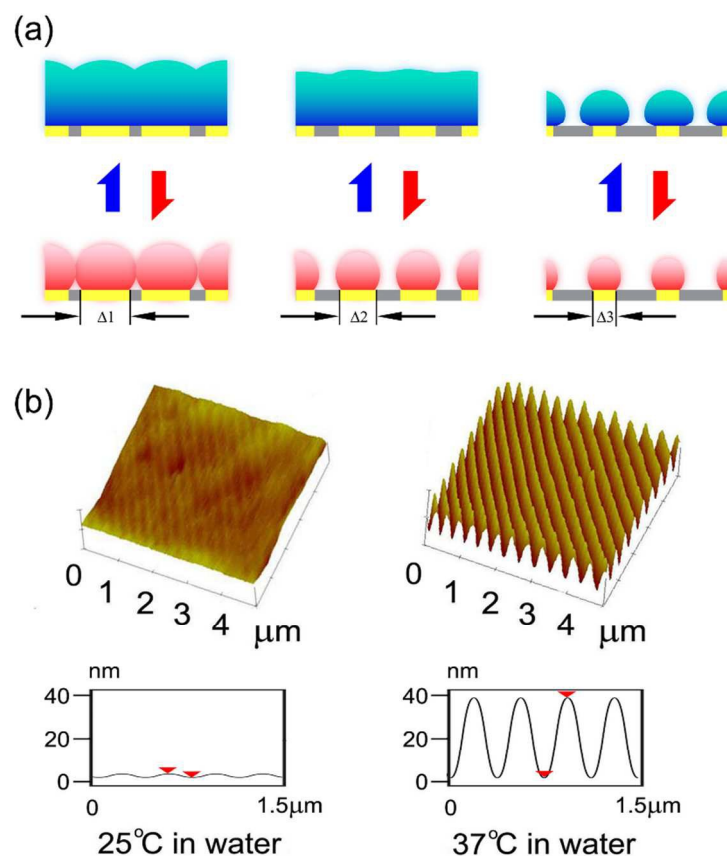


Figure 6. (a) Schematic representation of contour plots of nanopatterned polymer brushes with varying stripe width (Δ), $\Delta_1 > \Delta_2 > \Delta_3$. (b) Contact-mode topographical AFM image of nanopatterned PNIPAAm brushes under different conditions. The corresponding value of the peak-to-valley dimension (PVD, *i.e.*, the vertical distance between red arrows) is 1.6 ± 0.5 nm (at 25°C in water) and 38.0 ± 1.5 nm (at 37°C in water). [Adapted from Ref.⁸ with permission, Copyright 2013, The Royal Society of Chemistry.]

3 Synthesis and Patterning Methods for NPBs

Over the last two decades, many techniques have been developed to fabricate nanometer-scale patterned polymer brushes. The advances seen in this area have been enabled by progress both in patterning and polymerization techniques as we outline below. In *direct patterning* the polymer itself is

patterned, either through direct “writing” of the polymer on the surface or through ablation of a pre-formed polymer brush. In *indirect patterning* an initiator is patterned in some manner or immobilized onto nano-textured substrates, followed by *in situ* polymerization.

3.1 Direct patterning methods

3.1.1 Scanning probe lithography (SPL)

SPL encompasses a series of techniques including scanning tunneling microscopy (STM), atomic force microscopy (AFM), or scanning electrochemical microscopy (SECM) that all use sharp scanning tips to fabricate nanometer-scale features on surfaces. Advantages of SPL include its simplicity, versatility, and the ability to form precise, arbitrary spatial features while providing a method for imaging of structures *in situ*.^{38, 39} Next we highlight some examples of SPL to directly pattern as-prepared polymers with several different approaches, illustrated in **Figure 7**.

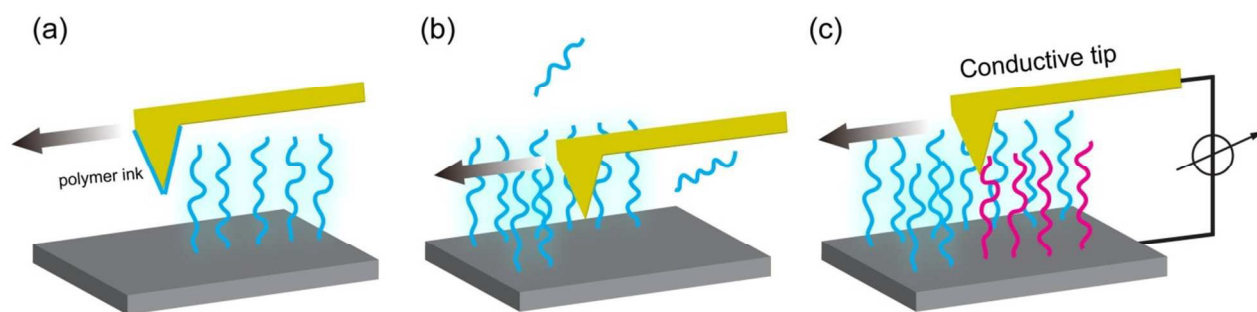


Figure 7. Direct patterning of polymer brushes using scanning probe lithography. (a) Deposition of polymers on the substrate by dip pen nanolithography, enabled by heating the cantilever probe to the polymer melting temperature.⁴⁰ (b) AFM nanoshaving of a polymer brush covered a substrate surface.⁴¹ (c) Field-induced, electrochemical removal of polymer brushes.⁴² [Adapted from Ref.^{40,41,42}]

Dip-pen nanolithography (DPN) uses an AFM tip as a nib to directly “write” functional molecules onto a solid substrate in contact mode (**Figure 7a**). DPN has thus been used to nanopattern small organic

molecules,^{43, 44} biomolecules,⁴⁵ or polymers^{40, 46, 47} onto inorganic supports such as gold and silicon wafers. For example, dendrimers of polyamidoamine or polypropylene imine have all been used as “inks” to write nanostructures with 100 nm features (~20 dendrimer molecules) on a silicon surface with the size of the pattern feature being dependent on the molecular weight of the dendrimer.⁴⁷ Stable nanopatterns of conducting polymers, including self-doped sulfonated polyaniline and doped polypyrrole, have been deposited on charged silicon surfaces *via* DPN using electrostatic interactions as a driving force.⁴⁰

A variety of modified DPN techniques have also been developed. For example, electrochemical polymerization at the AFM tip/substrate interface has been used to synthesize poly(3,4-ethylenedioxy-thiophene) polymer brushes *in situ*, creating nanostructures with lateral dimensions of less than 100 nm on semiconducting and insulating surfaces, thus enabling the fabrication of electronic nanodevices.⁴⁶ In thermal-DPN a solid polymer is melted into an ink by a heated probe and written directly onto a substrate.⁴⁸ Patterns fabricated using thermal-DPN are often more uniform and dense than those created using solvents.

AFM tips can not only be used as “nano-pens” to write polymers onto a surface, but also as “nanoshavers” to ablate regions of preformed polymer films⁴⁹ (**Figure 7b**). For example, well-defined patterns of the conducting polymer poly(3,4-ethylenedioxythiophene):poly (4-styrenesulphonate) were obtained by AFM nanoshaving at high applied normal force on both rigid and flexible substrates with 50 nm resolution. The scratched nanometer channel shows excellent performance in organic transistors with a low voltage and negligible short-channel effect.⁴¹ Due to the different chemical properties of substrate and polymer layer, site-selective immobilization of dyes or proteins on the patterned surfaces can also be

performed.^{49, 50}

Conductive AFM, in which hydrophilic polymer brushes tethered on a conductive substrate are ablated using an electrochemical reaction between the tip and substrate, has been used to create patterns of poly(oligo(ethylene glycol) methyl methacrylate) (POEGMA), and other polymer brush thin films (**Figure 7c**).⁴² During patterning a voltage was applied between the tip and the conductive substrate, which were separated by the polymer brush thin film. Using this method, it is possible to locally change the surface chemical composition of the polymer brushes in the patterned regions.

3.1.2 Electron beam lithography (EBL)

EBL writes patterns in thin films of electron sensitive material using a finely focused (sub-micrometer diameter) electron beam (e-beam). This method can be used in a single-step approach to directly generate patterns of polymer brushes as small as 50 nm on oxide surfaces.⁵¹ This technique requires a polymer that is e-beam scissile, such as a polymethacrylate. Furthermore, diblock copolymer brushes, with an upper layer that is not ablated by e-beam (*e.g.*, polystyrene, PS), and an lower layer that is e-beam- scissile (*e.g.*, poly(methyl methacrylate, PMMA), can be subjected to an e-beam to regio-selectively degrade the PMMA, while simultaneously cross-linking the overlying PS, producing nanochannels after developing with proper solvent to remove PMMA fragments (**Figure 8**).⁵²

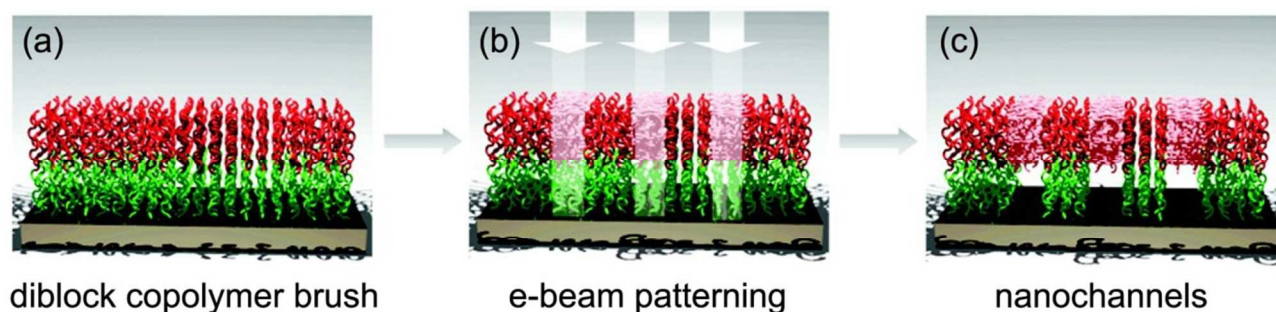


Figure 8. An illustration representing the fabrication of nanochannels based on nanopatterned diblock

copolymer PMMA-*b*-PS brushes. (a) The diblock brushes before patterning. (b) The diblock brushes after e-beam exposure. (c) The patterned diblock brush after development. [Reprinted from Ref.⁵² with permission, Copyright 2010, American Chemical Society.]

3.1.3 Photolithography

Photolithography (PL) using ultraviolet light (UV) is widely used to fabricate nanostructures by ablative patterning. Scanning near-field photolithography (SNP) utilizes a scanning near-field optical microscope coupled to a laser to initiate photochemical reactions with nanoscale spatial resolution.^{53, 54} For example, polymer films of plasma-polymerized tetraglyme (PP4G)⁵⁵ or POEGMA⁵⁶ were directly patterned in this way, resulting in features as small as 200 nm. UV-interferometric lithography (IL; see also **Section 3.2.3**) can be used to generate periodic patterns of azobenzene-group-containing poly(methyl acrylic acid) (azo-PMAA) brushes. These azo-PMAA brushes showed a strong response upon UV irradiation, which induced a photomechanical scission process that resulted in parallel interference patterns.^{57, 58}

3.2 Indirect patterning strategies: combining nanolithography and surface initiated polymerization

Surface initiated polymerization (SIP) can overcome some of the limitations imposed by patterning NPBs directly from preformed polymer. Destructive techniques in particular are often limited by the inability to completely remove the entangled polymer from the surface. In addition, direct patterning methods using incident electromagnetic radiation are only applicable to polymers that either assemble or degrade at specific energies.

In SIP-based patterning, initiators are (i) directly patterned, or (ii) ablated from uniform surface-immobilized initiator layers, which are formed by either chemisorption (covalent attachment) of small molecules or physisorption of macroinitiators onto the substrates. For the chemisorption strategy, the most frequently used method is based on self-assembly of ω -substituted alkyl thiols (for gold surfaces) or silanes (for oxide (*e.g.*, silica) surfaces), or by directly coupling small molecules that contain end groups with initiation activity, such as 2-bromoisobutyryl bromide or its analogues.^{16, 59}

In the physisorption strategy, a pre-synthesized polymer with initiator groups (*i.e.*, a macroinitiator) can be immobilized onto the substrate surface by spin-coating,⁶⁰ chemical vapor deposition,⁶¹ layer-by-layer deposition,⁶² or electrostatic adsorption.⁶³ These patterned initiators can subsequently serve as templates for polymerization, resulting in well-defined NPBs. The same nanolithography techniques described above for direct patterning can also be used and combined in indirect patterning for the creation of more complex architectures.

Recently developed techniques for SIP allow for direct control of the polymerization reaction kinetics, which results in brushes with a narrow molecular weight (MW) distribution and uniform height.⁶⁴⁻⁶⁶ Among different SIP methods, surface-initiated atom transfer radical polymerization (SI-ATRP) developed by Matyjaszewski *et al.*, has been widely considered to be an extremely versatile, accessible and robust technique to grow polymer brushes.⁶⁷ SI-ATRP provides many advantages including simple experimental setups, readily available initiators and catalysts that can be used in a range of solvents, allowing precise control over final polymer brushes with complex compositions and architectures (*e.g.*, block, gradient, inorganic/organic hybrid, and bioconjugate).⁶⁸ However, conventional SI-ATRP methods also suffer several drawbacks such as requirement of a relatively large

amount of a transition metal catalyst (usually based on copper) and a completely inert atmosphere for polymerization.⁶⁹ Therefore, considerable attention has been paid to developing ATRP variants that avoid these limitations.⁶⁸ A typical example is activator regenerated by electron transfer (ARGET)-ATRP, in which the oxygen-sensitive Cu(I) catalyst species are generated *in situ* from oxidatively stable Cu(II) species by the action of reducing agents within the polymerization reaction system.⁷⁰ The distinguishing advantages of ARGET-ATRP are that (i) the amount of copper can be reduced to only a few ppm and (ii) the reaction can tolerate limited amounts of oxygen.^{71, 72} Surface-initiated ARGET-ATRP from various material surfaces has been performed without the need for any deoxygenation,⁷³⁻⁷⁵ providing simplicity and accessibility for fabrication of NPBs. Besides SI-ATRP, other controlled SIP techniques, including surface-initiated reversible addition-fragmentation chain transfer polymerization (SI-RAFT)⁷⁶, surface-initiated photoiniferter-mediated polymerization (SI-PIMP)⁷⁷, surface-initiated nitroxide-mediated polymerization (SI-NMP)⁷⁸, surface-initiated ring opening metathesis polymerization (SI-ROMP)⁷⁹, and surface-initiated living anionic/cationic polymerization^{80, 81}, have also been applied to graft well-defined polymer brushes on surfaces. Several excellent reviews have detailed these polymerization mechanisms and their use in the synthesis of polymer brushes.^{1, 16-18, 59, 82-84}

3.2.1 Direct scanning probe lithography (SPL)

As is the case for direct patterning of polymers, SPL is a versatile and effective way to pattern initiator molecules. For example, DPN can be used to transfer thiol-functionalized initiator molecules from an AFM tip to a gold substrate,⁴⁴ where they serve as initiators for subsequent, localized polymerization.^{85, 86} Pattern precision can be increased by using DPN to pattern gold nanowires as small as 20 nm onto a silica surface, followed by incubation with thiol-functionalized initiator and subsequent

polymerization. This method has been used to produce nano-“hedges” of poly(methyl acrylic acid) (PMAA).⁸⁷

On the other hand, destructive methods, such as nanoshaving, can also be used to pattern initiators. For example, an AFM tip was used to selectively remove a preformed self-assembled monolayer (SAM) of methyl-terminated 1-octadecanethiol (ODT) on gold substrates, after which the gaps containing freshly exposed gold surfaces were backfilled by self-assembly of the thiol-substituted initiator (ω -mercaptoundecyl bromoisobutyrate). This technique has been used to great effect to produce PNIPAAm brushes with features down to 300 nm.^{88, 89}

Dip-pen nanodisplacement lithography (DNL) combines the attributes of DPN and nanoshaving to yield high resolution patterns (with feature sizes as small as 25 nm) of initiator molecules on a surface (**Figure 9a**).⁹⁰ After polymerization, three-dimensional polymer nanostructures of poly(2-(methacryloyloxy) ethyltrimethyl ammonium chloride) (PMETAC) with well-defined composition, properties, and morphology can be formed (**Figure 9b**).⁹¹ Recently, this technique has been parallelized, using a multiple AFM tip-array, and is able to fabricate patterns over a macroscopic area, while maintaining high resolution.⁹²

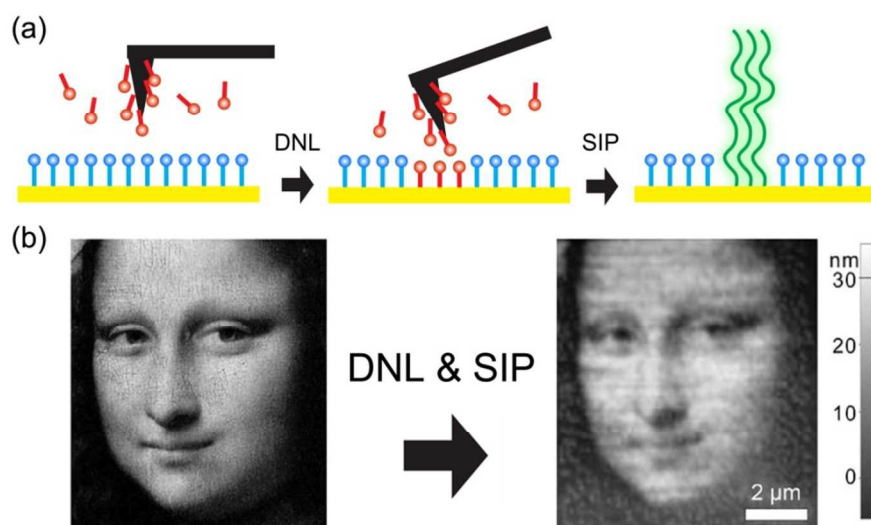


Figure 9. (a) Schematic illustration of the fabrication of NPBs produced by DNL and SIP. (b) Gray-scale digital photograph (left) and AFM topographic (right) image of the Mona Lisa obtained from PMETAC brushes. [Adapted from Ref.⁹¹ with permission, Copyright 2011, Wiley-VCH.]

A conductive AFM tip can be used to selectively oxidize surface-immobilized organic precursors and anodize the silicon underneath by applying a bias voltage to the substrate; the ablation and anodization are then followed by immobilization of initiator molecules on the oxidized regions. A typical example is reported by Lee *et al.*, in which nanopatterns of two chemically different polymers (poly(cyclooctatetraene) or poly(5-ethylidene-2-norbornene)) were fabricated on a single substrate by step-and-repeat anodization lithography followed by surface initiated ring-opening metathesis polymerization (SI-ROMP) (**Figure 10**).⁹³ In another example, octadecyltrichlorosilane (OTS) monolayers were locally oxidized by an AFM tip to generate silicon oxide nanopatterns, which served as a site-specific anchoring platforms for further functionalization of initiators and grafting of polymer brushes.⁹⁴

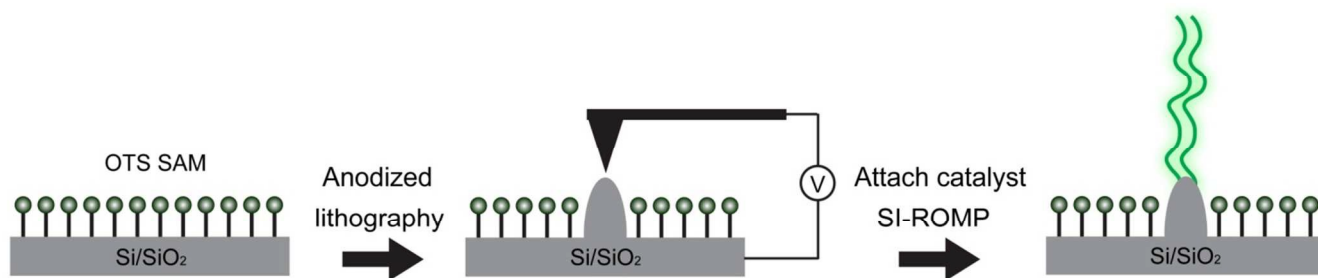


Figure 10. Schematic illustration of the fabrication of NPBs by anodized lithography and SI-ROMP.

[Adapted from Ref.⁹³ with permission, Copyright 2006, Wiley-VCH.]

3.2.2 Electron beam lithography (EBL)

Bombardment of a substrate with a high energy electron beam can be used to form a pattern by decomposing initiator molecules immobilized on its surface.⁹⁵ Unlike polymers, initiators are typically more susceptible to degradation during EBL. Alternatively, EBL can be used to pattern the substrate used for initiator immobilization. For example, using PMMA as an e-beam sensitive resist layer, lift-off EBL was used to fabricate gold patterns on a silicon substrate. The resultant patterns were functionalized with thiol-functionalized initiators for further polymerization (**Figure 11**).^{36, 96} Additionally, techniques combining lift-off EBL and gas-phase silanation have been used to obtain nanopatterns of polymer brushes on silicon substrates with features as small as ~ 25 -nm.^{9, 97, 98}

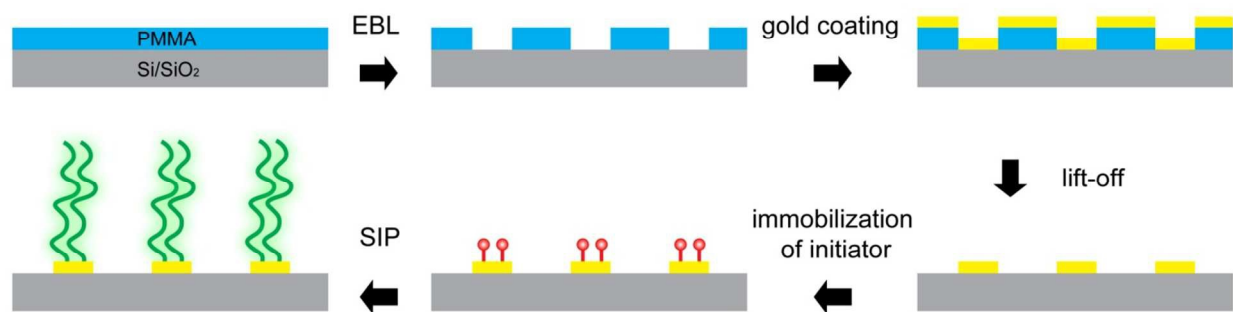


Figure 11. Schematic illustration of the fabrication of NPBs by lift-off EBL and SIP. [Adapted from Refs.^{36, 96}]

A variation on EBL, electron beam chemical lithography (EBCL), has been developed to achieve nanopatterns with specific chemical functionalities. For example, electron irradiation of aromatic SAMs of 4'-nitro-1,1'-biphenyl-4-thiol (NBT) results in selective and quantitative reduction of the nitro functionalities to amines, while the aromatic biphenyl groups dehydrogenate and crosslink.⁹⁹ The newly created amine groups can be subsequently functionalized through standard chemical reactions, including

those incorporating biologically relevant molecules or other functional macromolecules. EBCL has been used to create features as small as 50 nm.¹⁰⁰ EBCL can also be used to fabricate NPBs by incorporating chemical and photochemical initiators on a surface, followed by SI-ATRP¹⁰¹⁻¹⁰³ or surface-initiated photopolymerization (SIPP)^{99, 100} (**Figure 12**). The density of surface immobilized initiator is controlled by the e-beam dose in the EBCL process, so that NPBs with well-defined grafting gradients can be created. Major limitations to widespread use of this particular technique for initiator patterning are (i) that the precursors may not be commercially available, and (ii) that the amine generating reaction requires intensive e-beam irradiation. These limitations can be overcome using gold-thiolate SAMs made from dodecanethiol as resists. Because the gold-thiolate bond is energetically labile (it can be disrupted using UV irradiation), patterning can be performed with lower irradiation doses. The patterns produced can then be exposed to alkanethiols with reactive ω -substitutions (such as amines or carboxylate) and subsequently coupled with initiators for SIP.¹⁰⁴

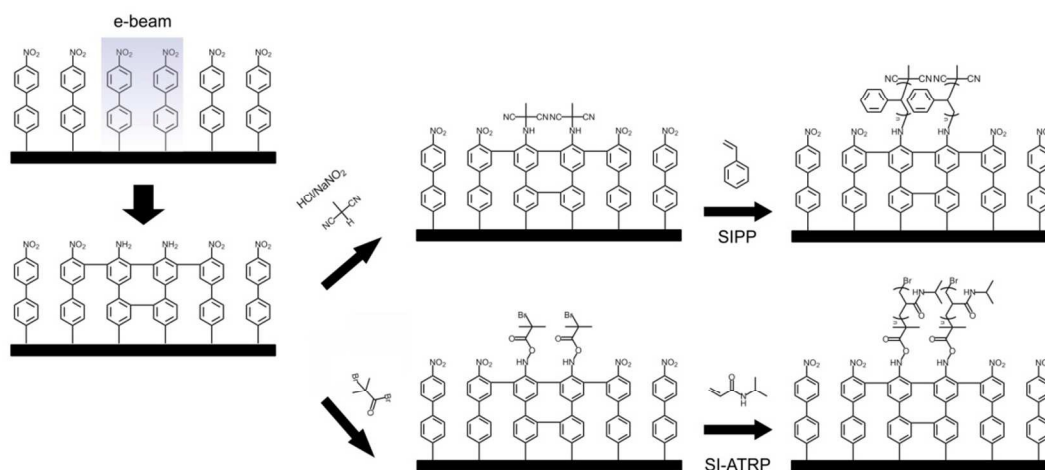


Figure 12. Schematic illustration of the fabrication of NPBs (PS or PNIPAAm) by EBCL and SIP (SIPP or SI-ATRP). [Adapted from Refs.⁹⁹⁻¹⁰³]

EBCL techniques are also limited in their utility because they require a multi-step procedure of initiator immobilization, structuring, and functionalization for the final SIP to produce NPBs. These limitations can be alleviated using a straightforward method for producing structured polymer brushes of controlled morphology by means of electron-beam-induced carbon deposition (EBCD).¹⁰⁴ In this method, a stable ultrathin template layer of carbonaceous material is locally deposited on an inorganic substrate by means of a focused e-beam, followed by direct photografting of vinyl monomers on the template. EBCD is a general method for the fabrication of stable polymer brush nanostructures on a broad variety of substrates without the need of specific surface chemistry.¹⁰⁴⁻¹⁰⁷

3.2.3 Interference photolithography (IL)

IL is a facile and high-throughput technique to provide periodic-nanopatterns over relatively large areal scales.¹⁰⁸ A prototypical IL apparatus is shown in **Figure 13**. During this simple IL process, a coherent laser beam is split into two beams. The top beam impinges on a mirror and reflects down to the substrate, while the other beam directly illuminates the substrate, yielding a sinusoidal light intensity distribution (*i.e.*, and interference pattern) on the substrate surface with a period of $\lambda/[2(\sin \theta/2)]$, where λ is the wavelength of laser beam and θ is the interference angle. This technique has been widely used for the fabrication of nanoelectronic, nanofluidic, and nanophotonic devices, and more recently, for patterning of initiators for NPB.¹⁰⁹⁻¹¹² In contrast to SPL and EBL, IL can be used to rapidly create patterns over relatively large ($\sim\text{cm}^2$) surface areas, therefore, shortening patterning time and increasing throughput. For example, UV IL can also degrade/deactivate monolayers of initiators immobilized on silicon substrates.^{111, 112} While most studies that have used IL to fabricate NPBs have formed simple patterns (*e.g.*, arrays of straight lines), it is possible to use interference of multiple laser beams to form

arrays of many types of geometrical nanoscopic objects using holographic approaches.^{108, 113}

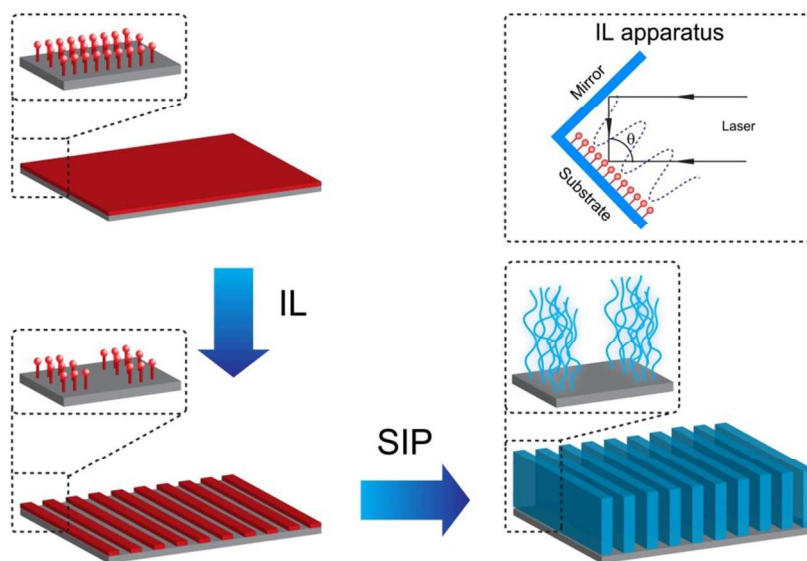


Figure 13. Schematic of preparation of nanopatterned brushes by IL and SIP. First, nanopatterns of ATRP initiators are fabricated *via* interferometric lithography (IL). Second, brushes (*e.g.*, PNIPAAm) are grafted from the nanopatterns of ATRP initiators. [Adapted from Ref.⁸]

IL can also easily create gradients of features that would normally be time-consuming to produce using single beam methods. The sinusoidal light intensity distribution generated by interference patterns creates similarly shaped concentration gradients of active initiators on the surface. These gradients are then propagated in the surface density and, sometimes, length of the polymer chains. For example, PMMA brushes synthesized with nanoscale gradients in grafting density were prepared by UV-IL from a pre-patterned photoinitiator layer, in which the high energy UV light decomposed the initiator only in sufficiently illuminated areas.¹¹¹ We routinely use UV-IL to selectively photo-degrade monolayers of ATRP initiators and conduct polymerization from IL-patterned initiators to achieve nanopatterns of thermo-responsive PNIPAAm brushes (**Figure 13**), which can then be employed in a

variety of applications, as discussed below.^{8, 25-28} Alternatively, irradiation of a polymer substrate with electrons or photons can directly generate reactive radicals, which can themselves serve as initiators for polymerization from surfaces.¹¹⁴⁻¹¹⁶

3.2.4 Nanoimprint lithography (NIL)

NIL is a simple and versatile nanopatterning technique that is able to produce three dimensional (3D) patterns with features as small as tens of nanometers.¹¹⁷⁻¹²⁰ As shown in **Figure 14**, typical NIL process for fabrication of NPBs requires two steps. The first step uses nanocontact methods to create a photopolymer mold, which imbeds functional molecules (inimers) with both initiator and monomer moieties into the desired pattern. In the second step, SIP is used on the exposed reactive sites to achieve polymer patterns.¹²⁰

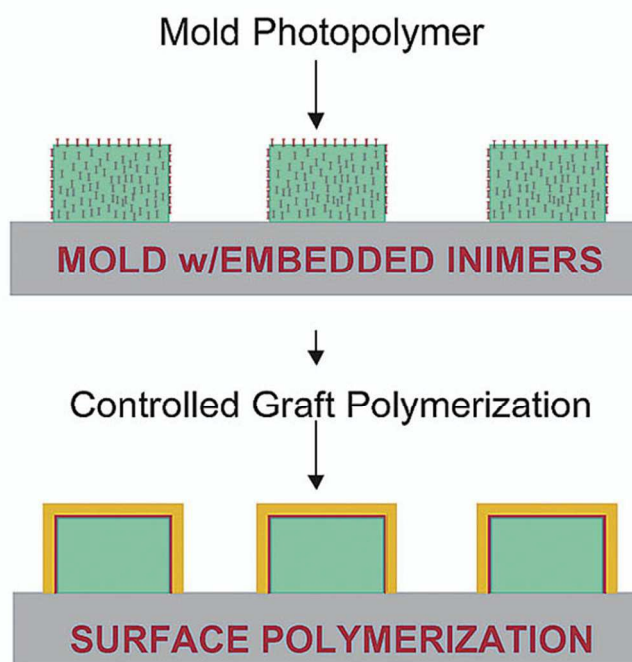


Figure 14. Schematic illustration of the fabrication of NPBs by NIL and SIP. [Reprinted from Ref.¹²⁰ with permission, Copyright 2003, American Chemical Society.]

3.2.5 Capillary force lithography (CFL)

CFL is a large-area patterning technique, which uses soft lithography to generate a mold, typically from polydimethylsiloxane (PDMS).^{121, 122} The PDMS mold, nanopatterned using similar techniques as those employed for NIL, is placed on the polymer film, which is then heated above the glass-transition temperature of the polymer. The capillary forces drive the melted polymer into the void space of the channels defined by the mold, thus generating a negative replicate. This method has been used to create patterned binary polymer brushes by the combination of CFL and SIP (Figure 15).¹²³ Like NIL, this does not require irradiation of either the substrate or the polymer, and has been used to produce feature sizes on the order of 100 nm.

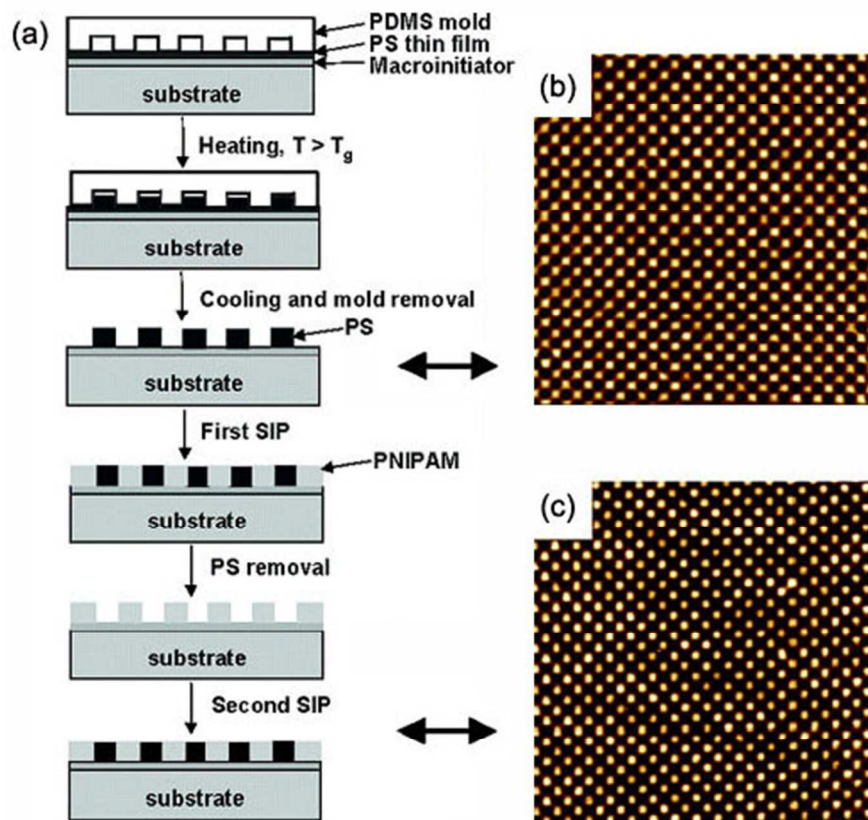


Figure 15. (a) Schematic illustration of the fabrication of binary, orthogonal NPBs by CFL and SIP. (b)

AFM image of a PS pattern created on top of a macroinitiator surface (image: $20 \times 20 \mu\text{m}$). (c) AFM

image of PNIPAAm brush pattern created by CFL and SIP ($20 \times 20 \mu\text{m}$). [Reprinted from Ref.¹²³ with permission, Copyright 2006, American Chemical Society.]

3.3 Polymer brushes grafted from nano-textured substrates

The previous two sections discussed NPSs fabricated on planar substrates. Perhaps the simplest way to form an NPB is by grafting polymer chains at a surface of a material with pre-existing, nanoscale textures or nanopatterned structures. Such nanotextured substrates include porous silicon (pSi),¹²⁴ silicon nanowire arrays (SiNWAs),¹²⁵ nanoporous anodic aluminum oxide (AAO),¹²⁶ or titanium dioxide nanotube arrays,¹²⁷ for example. Polymers can be either (i) directly immobilized on nanotextured substrates by a range of methods, including physisorption,¹²⁸ chemical vapor deposition,¹²⁹ layer-by-layer deposition,¹³⁰ and click-chemistry,¹³¹ or (ii) more commonly, grafted from initiator-functionalized substrates by SIP.^{30, 31, 132} The resultant polymer chains can be located on the topmost surface and/or inside nanopores. If the grafted polymers exhibit stimuli-responsive properties, the resultant NPBs can be used to dynamically control the wetting characteristics of such surfaces, the diffusional and convection-based transport through nanopores, or the adsorption within the porous materials (examples will be given in the application section below).

4 Applications of NPBs

Due to their various chemical functionalities, good mechanical and physical properties, and special topological features (*e.g.*, the commensurate length scales of the polymer brush height and the lateral patterning dimension), using the techniques discussed above, NPBs can be tailored to provide platforms

for a plethora of different applications. In this section, we highlight recent examples that used NPBs for (i) controlling surface wettability, (ii) patterning biomolecules, (iii) the investigation of cell-substrate interactions, (iv) controlling surface bioactivity, (v) controlled release of molecules from nanoporous materials, and (vi) other applications.

4.1 Controlling surface wettability

Wettability, particularly by aqueous media, is an important property of surfaces that has implications for the performance for a wide variety of applications, in both daily life and in industry.¹³³⁻¹³⁵ Two extremes of aqueous wettability of solid surfaces, superhydrophilicity (with a water contact angle (WCA) $<5^\circ$)¹³⁶ and superhydrophobicity (with a WCA $>150^\circ$)¹³⁷ have attracted considerable attention. The wettability of solid surfaces is typically governed by a combination of interfacial chemistry (which dictates interfacial free energy) and surface roughness at the micro- and nanoscale.^{138, 139} The introduction of nanotexture into solid surfaces can have a profound effect on their wettability as described theoretically by the Wenzel and Cassie-Baxter models.^{140, 141} Experimentally, this is illustrated by a flat silicon surface coated with a thin native oxide layer, which is hydrophilic with a WCA less than 20° ; the introduction of nanostructures (*e.g.*, by the formation of silicon nanowire arrays (SiNWAs)) will result in superhydrophilicity, *i.e.*, a WCA of $\sim 0^\circ$. On the other hand, after modification of SiNWAs with a hydrophobic layer, the low surface energy of the coating and the nanostructure of SiNWAs synergistically can generate a stable superhydrophobic surface.¹⁴² In recent decades, a number of works have demonstrated that nanotextured surfaces, modified by NPBs, exhibit unique wettability as compared with the corresponding smooth surfaces; readers who are interested may refer to several excellent reviews^{20, 143, 144}.

The use of external stimuli (*e.g.*, heat, light) to dynamically change and control surface wettability has been exploited in a number of areas, including microsystems, materials science, biotechnology and medicine.¹⁹ Such stimuli-responsive or “smart” surfaces with switchable interfacial properties can also be used to regulate the adsorption of biomolecules and adhesion of cells.^{145, 146} Several reports have shown that such changes in surface wettability in response to external stimuli can be greatly enhanced by nanoscale roughness¹⁴⁷⁻¹⁴⁹. For example, Lopez and coworkers grafted PNIPAAm brushes onto anodic aluminum oxide membranes (widely-available, nanotextured model surfaces) with varying pore sizes of 20, 100, and 200 nm.³² They found that the WCAs of these surfaces, both below and above the LCST of PNIPAAm in water, depended dramatically on the membrane’s pore size (and thus nanoscopic roughness). Increasing the pore size of the substrate led to a gradual decrease in the WCAs measured at temperature below the LCST and a dramatic increase in WCAs measured at temperature above the LCST (**Figure 16a**). Similarly, Yu and coworkers modified SiNWAs with PNIPAAm and systematically investigated the temperature-dependent wettability.¹³² Changes in temperature from 23°C to 37°C also lead to a significant change in wettability of SiNWA-PNIPAAm surfaces in air (from superhydrophilic (WCA ~0°) to strongly hydrophobic (WCA ~120°), as shown in **Figure 16b**). Interestingly, this surface remained superoleophobic in water with an oil CA over 140° regardless of temperature. This was attributed to the presence of water molecules trapped in the interstices of the SiNWAs. In another report, the dual responsive wettability of SiNWAs, grafted with poly(2-(dimethylamino)ethyl methacrylate) (PDMAEMA), was investigated (**Figure 16c**)¹⁵⁰. This surface shows trends in WCA in response to changes in pH and salt concentration. At pH 3, the surface is strongly hydrophilic, independent of ionic strength. In contrast, at pH 5 and above, the surface becomes more wettable with increasing ionic

strength.

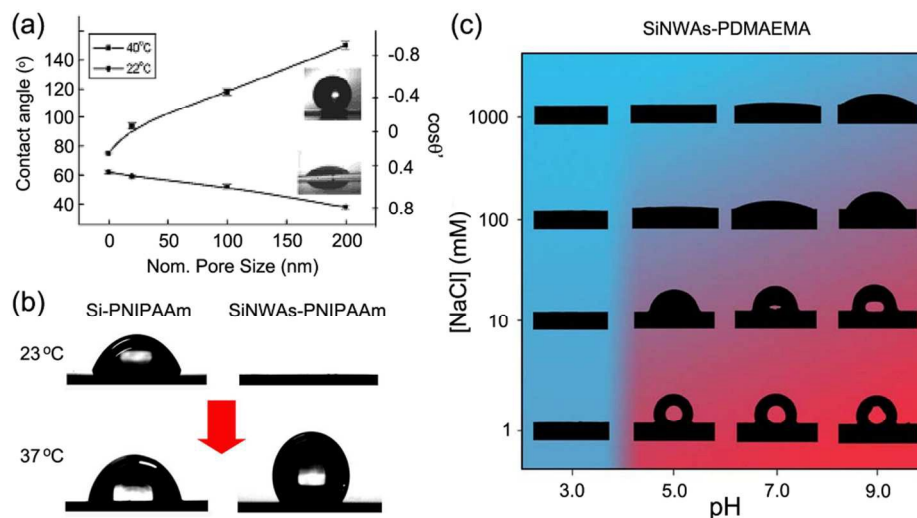


Figure 16. (a) Water contact angle (WCA) data (sessile drop) measured at 22°C and 40°C for PNIPAAm grafted to AAO surfaces with varying nominal pore size. (b) Typical contact angle images for (a) Si-PNIPAAm and SiNWAs-PNIPAAm surfaces at both 23°C and 37°C. (c) Influence of pH and NaCl on the WCA of SiNWAs-PDMAEMA surfaces. [Reprinted from Refs.^{32, 132, 150} with permission, Copyright 2004, American Chemical Society; Copyright 2011, The Royal Society of Chemistry; Copyright 2011, The Royal Society of Chemistry.]

4.2 Patterning biomolecules

Guidance the patterned adsorption of biomolecules onto solids with nanoscale resolution is useful in the fundamental study of biologically relevant processes on surfaces and in the development of advanced biochips and biosensors.¹⁵¹⁻¹⁵⁴ Using the techniques described in **Section 3**, biomolecules can be nanopatterned directly⁴⁵ or using pre-patterned surfaces with nanoscale features (*e.g.*, NPBs) as templates.¹⁵⁵⁻¹⁵⁷ Here, polymer brushes offer a number of advantages over other types of surface modification in controlling the adsorption of biomolecules on surfaces. For example, brushes of highly

hydrated polymers such as poly(ethylene glycol) (PEG), and its derivatives, or polyzwitterions are highly resistant to nonspecific protein adsorption, making these brushes excellent candidates for use in areas of a surface in which one wants to minimize biointeraction.^{158, 159} Furthermore, polymer brushes can be tailored to display high and controlled densities of protein ligands, both within the plane of the brush (using mixed brushes, for example) or along the polymers themselves.^{3, 160}

To decrease non-specific interactions, and thus increases selectivity, as well as signal-to-noise ratio, biosensors can benefit from the patterning of biomolecular receptors within a nonfouling matrix.^{159 161} For example, crosslinking of surface-grafted, amine-terminated PEG *via* e-beam lithography was used to create hydrogel nanoarrays with ~200 nm features on silicon substrates.¹⁶² The amine groups were then used to covalently link different proteins to the patterned substrate *via* *N*-ethyl-*N'*-(3-(dimethylamino) propyl) carbodiimide/*N*-hydroxysuccinimide (EDC/NHS) chemistry. Another example is the immobilization of proteins on reactive regions patterned by exposing protein-resistant PP4G⁵⁵ or POEGMA⁵⁶ brushes to UV light using SNP techniques. The UV light causes a loss of polyether units and the creation of aldehyde groups that can be used to immobilize proteins. As shown in **Figure 17**, bright lines are clearly distinguishable from the background, suggesting that NeutrAvidin conjugated, yellow-green fluorescent nanoparticles, strongly adsorbed to UV-exposed areas, while the unexposed regions retained their protein resistance.

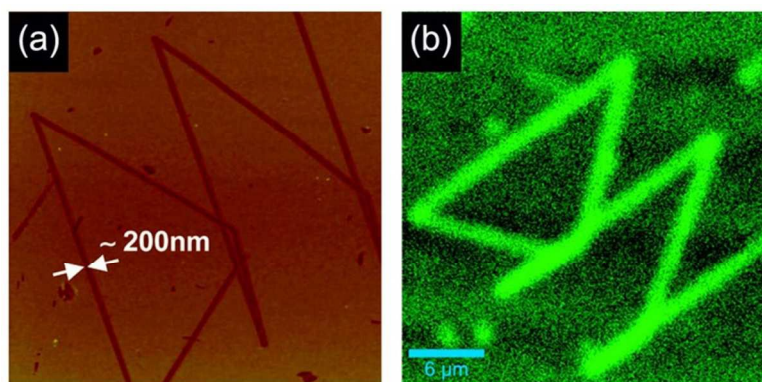


Figure 17. (a) AFM height image of a POEGMA brush sample that has been patterned using a scanning near-field optical microscope. (b) Fluorescence microscopy image of a similar sample following exposure to a solution of NeutrAvidin conjugated yellow-green fluorescent nanoparticles (40 nm). [Reprinted from Ref.⁵⁶ with permission, Copyright 2010, American Chemical Society.]

Biotin, a high affinity ligand for avidin and streptavidin, was conjugated to poly(glycidylmethacrylate) (PGMA) brushes that were grafted onto flexible fluoropolymer films and nanopatterned by a combination of UV-IL and radical polymerization. The resulting surfaces were used as nanoarray platforms for standard biotin-streptavidin assays.¹¹⁴ In another example, streptavidin nanopatterns were produced by biomolecular recognition of pre-patterned, biotinylated poly(L-lysine)-graft -poly(ethylene glycol) (PLL-g-PEG) brushes on Nb₂O₅ substrates, produced by a combination of NIL and lift-off molecular assembly. The resulting surfaces thus can serve as universal platforms for the immobilization of biotin-tagged biomolecules.¹⁶³

4.3 Investigation of cell-substrate interactions

Cell-substrate and cell-cell interactions play crucial roles in biotechnology and biology, and clearer understanding of these interactions is important to explain cell behavior *in vitro* and *in vivo*. From *in*

in vitro experiments, it is well known that cells respond to micro- and nano-features that have different chemistries and topographies.¹⁶⁴⁻¹⁶⁶ For example, mammalian cell function is partly directed by interactions with nanosized structures constructed from extracellular matrix (ECM), resulting in well-documented changes in adhesion, proliferation, migration, and gene expression.^{24, 167} Mammalian cells are also known to respond to nanoscale topographical features on synthetic substrates, *e.g.*, nanogrooves, nanopillars, and nanocolumns.^{23, 164, 168} Thus, nanostructured surfaces provide a controllable, *in vitro* platform on which to study cellular response to variables such as feature spacing and surface chemical cues, and to modulate such responses for biotechnological applications.^{23, 164} Furthermore, NPBs surfaces enable the study of cell-surface interactions with precise control and variation of biomolecule (*e.g.*, cell adhesion ligands, growth factors) concentration and accessibility and provide potent platforms for a broad range of biomedical applications, including tissue engineering, cell aggregate formation, and for various biological assays.^{166, 167, 169}

Polymer brush nanogradients have also been used to study cell-substrate interactions and to tailor cell adhesion on biomaterial interfaces.¹⁷⁰⁻¹⁷² For example, orthogonal gradient PHEMA brushes with gradually varying graft density (σ) and/or molecular weight (MW) were modified with the extracellular matrix protein, fibronectin (FN), to obtain a gradient density of FN on the surface.¹⁷³ Due to the protein-resistance of PHEMA, increases of σ and MW decreased FN coverage, which in turn decreased the adhesion density of osteoblastic MC-3T3 E1 cells cultured on this surface. Similarly, a PNIPAAm gradient, with a linear variation of thickness and covalently anchored on to a silicon substrate, affected attachment and detachment of HepG2 cells. A critical thickness range (20-45 nm) was found in which the cells could be attached and detached by temperature-induced phase changes.¹⁷⁴ These studies

demonstrate that surfaces nanopatterned with gradient polymer brushes can serve as useful platforms to study the effect of surface chemistry and topography on cell behavior.¹⁷⁵

4.4 Controlling surface bioactivity using nanopatterned stimuli-responsive polymer brushes

Stimuli-responsive polymers (SRPs) undergo conformational and/or chemical changes that are triggered by external stimuli, often within physiological ranges, and are thus of particular interest for developing active, nanostructured platforms on which to study biointerfacial interactions.^{176, 177} Among SRPs, PNIPAAm is a well-studied, thermally responsive polymer with a physiologically relevant, lower critical solution temperature (LCST) of $\sim 32^{\circ}\text{C}$ in water. When PNIPAAm is grafted to a surface, the LCST behavior translates into a change in wettability¹⁷⁸ and in polymer layer swelling.¹⁷⁹

Although most research to date has focused on applications of micropatterned, SRP brushes,¹⁸⁰⁻¹⁸² the focus is shifting to stimuli-responsive NPBs to exploit properties that are only available on the nano (and thus, molecular) scale. Investigation of the temperature-dependent swelling process of nanopatterned PNIPAAm brushes in water^{101, 102} revealed that as the temperature is increased from 25°C (below the LCST) to 40°C (above the LCST), a sharp decrease in polymer brush height occurs, which is attributed to water being expelled from the polymer brush layer. This temperature-induced change of brush conformation and swelling is reversible.^{183, 184} Although research on stimuli-responsive NPBs is still in its early stage, and emphasizes the nature and details of hydration transitions, the integration of nanopatterned SRP brushes into practical devices is being increasingly explored. For example, the reversible phase transition of PNIPAAm modified surfaces has been exploited to control the adsorption

and desorption of proteins.¹⁸⁵ Furthermore, thin, nanopatterned PNIPAAm layers, produced using thermal DPN, retained the ability of unpatterned PNIPAAm to reversibly bind and release bovine serum albumin (BSA) by temperature cycling through the LCST.⁴⁸

Inspired by the Monte Carlo simulations of Alexandros *et al.*¹², we have investigated the properties of patterned PNIPAAm brushes and exploited them to develop new platforms with switchable bioactivity.⁸ These nanopatterned PNIPAAm surfaces undergo a significant topographical change between 25°C and 37°C in aqueous environments (**Figure 18a**). At 25°C (below the LCST), the surface was relatively smooth, with barely noticeable nanopattern features, due to the lateral spreading of hydrated PNIPAAm brushes. However, upon increasing the temperature to 37°C (above the LCST), the polymer brushes collapsed and a distinct surface nanopattern became obvious. This temperature-triggered conformational change was repeatable for several cycles, thus enabling the thermally regulated concealment and exposure of molecules that were immobilized between the nanoscopic lines of PNIPAAm brushes.

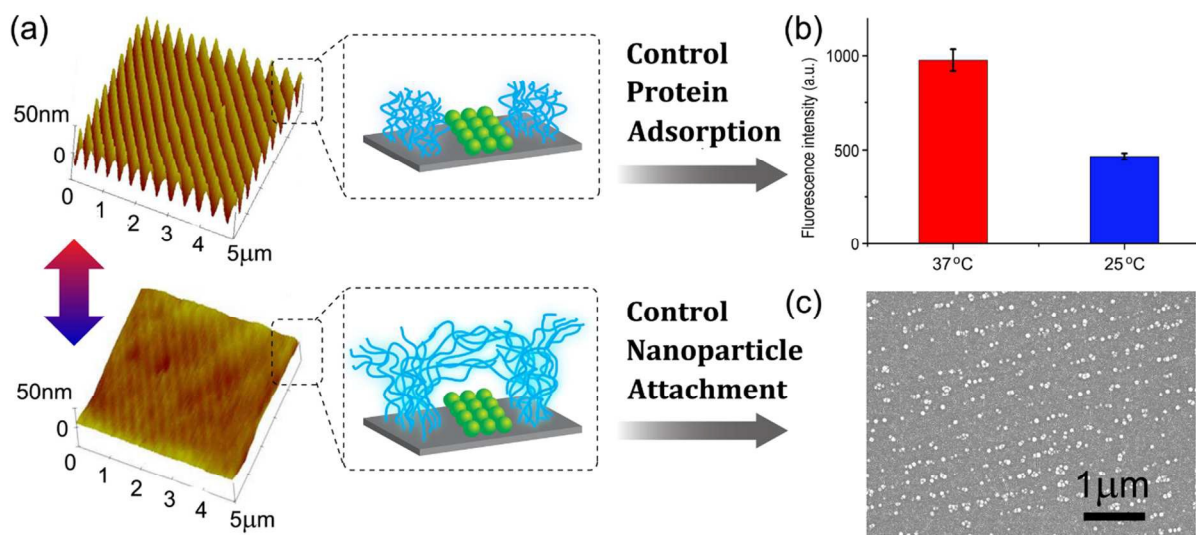


Figure 18. (a) Contact-mode topographical AFM images of nanopatterned PNIPAAm surfaces in water

at 37°C (upper) and 25°C (lower). This temperature-responsive conformational change can be used to expose or hide functional molecules immobilized in the polymer-free regions. (b) Adsorption of fluorophore-labeled streptavidin on nanopatterned PNIPAAm surfaces (after immobilization of BSA-biotin) at 37°C and 25°C. (c) SEM image of streptavidin-labeled nanoparticles adsorbed on nanopatterned PNIPAAm surfaces (after immobilization of BSA-biotin). [Adapted from Ref.⁸ with permission, Copyright 2013, The Royal Society of Chemistry.]

We demonstrated that the temperature dependent, conformational changes of PNIPAAm brushes in water can control access to proteins immobilized on nanoscopic, polymer-free regions of the substrate. This allows to reversibly switch the surface bioactivity between an “ON state” (above the LCST, the collapsed PNIPAAm chains exposes ligands adsorbed in areas between the brushes, for example) and an “OFF state” (below the LCST, the swollen PNIPAAm chains conceal the ligands). For example, because dense PNIPAAm brushes can be resistant to nonspecific protein adsorption both above and below the LCST,¹⁸⁵ biotin-labeled BSA (BSA-biotin) can be physisorbed into the PNIPAAm-free regions of the nanopattern and then exposed to with streptavidin (SA) above and below the LCST. As shown in **Figure 18b**, a marked decrease in SA binding was observed as the temperature decreased from 37°C to 25°C. This clear difference suggests that, at 25°C, biotin binding sites were effectively occluded by the extended PNIPAAm brushes, whereas at 37°C, biotin binding sites were made available by the dehydration and collapse of the nanopatterned PNIPAAm brushes.

Moreover, we found that the nanopatterned PNIPAAm brushes affected adsorption based on the size of the adsorbing species. For example, the adsorption ratio between 37°C and 25°C for SA (~2 nm) and

SA-labeled nanoparticles (SA-NPs, 40 nm) is 1.70 ± 0.15 and 3.34 ± 0.31 , respectively, suggesting an enhanced temperature dependence of biospecific adsorption for larger rather than smaller adsorbates. This difference might be due to the difference in steric limitations to diffusive transport for these adsorbates through the hydrated PNIPAAm brush overlayer. Scanning electron microscope (SEM) images clearly showed that almost all of the SA-NPs bound to the parallel interstices between the patterned polymer brushes (**Figure 18c**). These results suggest that nanopatterned, responsive polymer brush systems provide a facile means by which to dynamically control the diffusion limited adsorption of proteins and nanoparticles to engineered surfaces.

Expanding upon these results, and drawing on other work on interfacial interactions between PNIPAAm modified surfaces and microorganisms that established the use of PNIPAAm as a material that can exhibit triggered biofouling-release,¹⁸⁶⁻¹⁹² we developed nanopatterned PNIPAAm surfaces as a bifunctional platform with switchable antimicrobial activity and fouling-release capability, by integration of biocides into PNIPAAm brush nanopatterns.²⁶⁻²⁸ In three separate studies, three types of biocidal agents (a quaternary ammonium salt: dimethyloctadecyl [3-(trimethoxysilyl) propyl] ammonium chloride (QAS)²⁶, a hydrolase: lysozyme²⁷ and a light-activated singlet oxygen sensitizer: poly(phenylene-ethynylene) (PPE)²⁸) were physisorbed into the void spaces between PNIPAAm brush nanopatterns. We examined the attachment, killing and release of *Escherichia coli* on the nanopatterned PNIPAAm/biocide hybrid surfaces (**Figure 19**). At 37°C, the hybrid surface attracted *E. coli*; the biocides, exposed by the collapse of the PNIPAAm brush, killed the adhered cells. SEM examination of the killed bacteria indicated that their cell envelopes were severely damaged, resulting in loss of cellular integrity and function. Upon transitioning the temperature to below the LCST, the adhered dead bacteria

were released from the hybrid surfaces, which renders the hydrated brush surface unfavorable for cell adhesion, and regenerated the biocidal function by releasing dead cells and their debris from the contact-active biocides. This cycle of killing and release could be repeated several times. This platform represents a new paradigm for biocidal surfaces, as they can be reset and thus diminish the problem of fouling and inactivation that plagues most contact-biocidal surfaces.

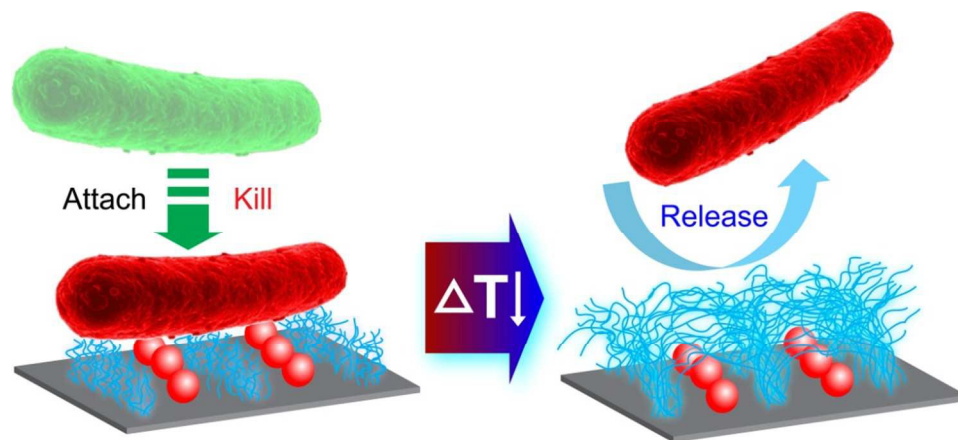


Figure 19. Schematic of attachment, killing and thermally triggered release of bacteria on nanopatterned hybrid PNIPAAm/biocide surfaces. [Reprinted from Ref.²⁷ with permission, Copyright 2014, The Royal Society of Chemistry.]

We conducted similar experiments with stimuli-responsive NPBs to control the attachment and detachment of mammalian cells.²⁵ PNIPAAm-coated surfaces have previously been applied as cell-culture substrates that enable the reversible adhesion and detachment of cells.^{193, 194} Because cells can be detached from PNIPAAm without mechanical or enzymatic disruption, nanopatterned PNIPAAm brushes have potential to release adherent cell types for subsequent analysis, expansion or regenerative medicine applications. However, one limitation of this approach has been the critical dependence of cell attachment and detachment on a narrow range of optimal thickness (20-45 nm) of the PNIPAAm

layer.¹⁷⁴ On thicker PNIPAAm brushes, cells did not adhere at 37°C, presumably because polymer chains in the outermost surface regions remained sufficiently hydrated, and, thus, repulsive. On thinner PNIPAAm brush layers, however, cell release was observed to be significantly less effective upon transition to temperatures below the LCST. We found that this limitation may be overcome by integration of cell-adhesive ligands (*e.g.*, a common extracellular matrix protein, fibronectin) into nanopatterned PNIPAAm surfaces.²⁵

In summary, the examples provided here demonstrate that conformational changes in stimuli-responsive NPBs provide a general strategy for controlling surface activity and biospecific recognition at nanoscopic levels. This may be useful for a variety of practical applications in the biomedical and biotechnology fields.

4.5 Controlled release from nanoporous materials

Grafting of polymer brushes on nanotextured surfaces is a simple way to form a NPB. When SRPs are grafted onto nanoporous substrates, the molecular conformational changes of SRPs in response to external stimuli can endow these hybrid material systems with unique “gating” functionality, *i.e.*, the pores can be opened or closed (or the effective pore size can be modulated) depending on whether the SRPs are in collapsed or extended conformational state. This dynamic property has been used to control the diffusional permeation of molecules through nanoporous membrane materials^{33, 195} or for on-demand release of drugs.^{30, 196, 197}

Nanoporous materials such mesoporous silica, porous silicon (pSi) and anodic aluminum oxide (AAO) have been explored as materials for controlled uptake and release applications due to their good mechanical stability, tailorable surface chemistry, and their high surface area. For example, Lopez and

coworkers modified mesoporous silica particles with PNIPAAm, such that the size and surface energy of pores can be externally and reversibly controlled to dynamically modulate the transport of aqueous molecular solutes.²⁹ Extending such approaches, Chu and coworkers used SI-ATRP of PNIPAAm to fabricate a thermo-responsive, gating AAO membrane.¹⁹⁵ As shown in **Figure 20a**, above the LCST, the PNIPAAm chains grafted in the membrane pores are collapsed, thus opening the pores; while below the LCST, the grafted PNIPAAm chains are hydrated, thus effectively reducing the size of the pores. This temperature-induced change of pore size led to a reversible and reproducible thermo-responsive diffusional permeation of vitamin B12 through the membrane. Similarly, PNIPAAm modified pSi films were shown to have high drug loading and excellent temperature-controlled drug release.³⁰ Modulation of the temperature around the LCST significantly altered the release rate of camptothecin from hybrid films (**Figure 20b**). We note that the conformational change in surface-grafted polymer chains is not limited to thermo-responsive PNIPAAm, but can be extended to other SRP systems including electrical-responsive polymers such as polypyrroles³³ and pH-responsive polymers such as poly(acrylic acid)¹⁹⁸ and poly(2-N,N-dimethylamino ethyl methacrylate)¹⁹⁹.

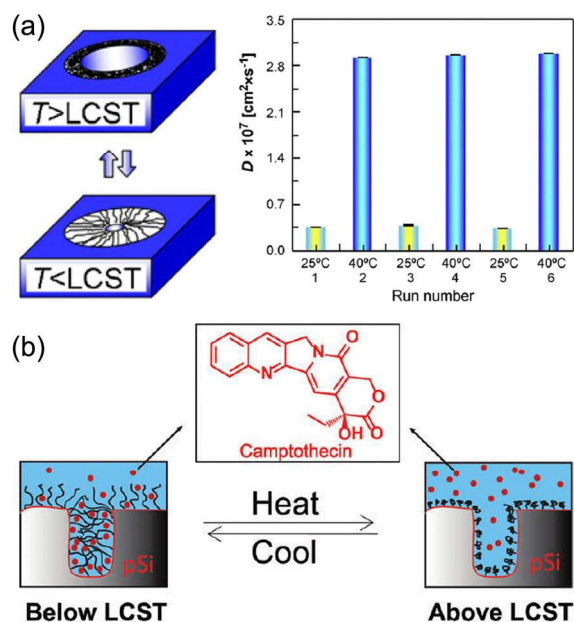


Figure 20. (a) Reversible thermo-responsive diffusional permeation of vitamin B12 across PNIPAAm-modified AAO membranes. (b) Schematic showing the drug release mechanism from a PNIPAAm modified pSi film. [Reprinted from Ref.¹⁹⁵ and Ref.³⁰ with permission, Copyright 2009, Elsevier; Copyright 2011, American Chemical Society]

4.6 Other applications

In addition to the applications discussed above, NPBs are finding utility in a variety of areas. For example, NPBs can provide the experimental platforms to investigate the conformational changes of polymer chains under nanoscale confinement. This opens up the opportunity to better understand polymer chains and solvation dynamics, and provides a useful tool for the design and fabrication of polymeric and bio-macromolecular nanostructures on surfaces.^{9, 11, 13} Moreover, patterned polymer brushes can serve as robust barriers to a range of chemical etchants, which is of significant importance for the fabrication of microelectronic and photonic devices.^{200, 201} Advances in the fields of

molecular-scale electronics, magnetic storage, optoelectronics, and biotechnology, all depend increasingly on the ability to fashion materials with precise control of feature size and functionality. Large-scale and high-throughput surface patterning with polymers is of fundamental importance not only to the microelectronics industry, but also to other areas of modern technology, including the fabrication and function of nanodevices such as nanofluidic platforms,²⁰² actuators,²⁰³ and biosensors.²⁰⁴

5 Summary and Perspective

Various techniques have been developed to fabricate NPBs on a wide range of substrate types, with each of these techniques has its advantages and limitations. Even in the absence of resource limitations, the optimal method of patterning for a particular application, the balance between pattern resolution, flexibility and pattern throughput (*i.e.*, patterning rate) must be taken into account. For example, while photolithography is a convenient technique for patterning polymer brushes over large areas at high throughput, it is difficult to get submicrometer feature sizes due to inherent diffraction limitations. The resolution problem has been solved through use of scanning near-field photolithography, which can be used to obtain feature sizes on the order of nanometers. However, this approach requires is inherently slow. Similar limitations also hinder the widespread application of EBL. While IL, CFL, and NIL are facile methods to pattern polymer brushes over large area (several cm² with submicrometer resolution); these methods suffer from less flexibility in nanopatterned polymer feature shapes, imposed by the means by which master patterns are generated. Although the recent rapid development of multiple robust methods for SIP has provided many chemistries for producing NPBs of homopolymer, random copolymers and block copolymers, development of NPBs into future areas of application will require advances that simultaneously improve patterning efficiency, versatility, and cost effectiveness, making

such processes suitable for industrial implementation.

Complex nanopatterns of polymer brushes, which exhibit well-defined feature dimensions and controlled chemical and physical properties, can pave the way for a new generation of advanced materials and devices. These nanostructured systems not only can be used as passive resists for fabrication of nanodevices in the semiconductor industry, but can also serve as carrier matrices for immobilization of functional biomolecules, including proteins, peptides, and nucleic acids. Patterned polymer brushes with nanoscopically defined architecture and chemical functionality are an ideal platform for immobilization of cell adhesion proteins and peptides to mimic local biological environments, which is of great importance for both the fundamental understanding of cell-cell and cell-matrix interactions and their manipulation. Combining nanofabrication and SRPs provides engineered, active surfaces in which the structures and functionalities of polymers at the nanoscopic scale can be modulated temporally, and thus endows these systems with great potential for basic research, biosensing, cell culture, and antifouling applications. Clearly, the applications of NPBs are still in the early stage of development; further development of nanofabrication and synthetic techniques will continue to enable widespread, practical applications of nanopatterned polymer brushes into the future.

Acknowledgments

This work was financially supported by the US Office of Naval Research (N00014-13-1-0828) and the US National Science Foundation's Research Triangle MRSEC (DMR-1121107). Q. Yu acknowledges financial support from the National Natural Science Foundation of China (21404076) and the Natural Science Foundation of Jiangsu Province (BK20140316). L. K. Ista acknowledges support by the

Defense Threat Reduction Agency (HDTRA-1-11-1-0004).

References

1. B. Zhao and W. J. Brittain, *Prog. Polym. Sci.*, 2000, **25**, 677-710.
2. O. Azzaroni, *J. Polym. Sci., Part A: Polym. Chem.*, 2012, **50**, 3225-3258.
3. N. Ayres, *Polym. Chem.*, 2010, **1**, 769-777.
4. A. Olivier, F. Meyer, J. M. Raquez, P. Damman and P. Dubois, *Prog. Polym. Sci.*, 2012, **37**, 157-181.
5. T. Chen, I. Amin and R. Jordan, *Chem. Soc. Rev.*, 2012, **41**, 3280-3296.
6. X. Zhou, X. Liu, Z. Xie and Z. Zheng, *Nanoscale*, 2011, **3**, 4929-4939.
7. R. Ducker, A. Garcia, J. Zhang, T. Chen and S. Zauscher, *Soft Matter*, 2008, **4**, 1774-1786.
8. Q. Yu, P. Shivapooja, L. M. Johnson, G. Tizazu, G. J. Leggett and G. P. Lopez, *Nanoscale*, 2013, **5**, 3632-3637.
9. A. M. Jonas, Z. Hu, K. Glinel and W. T. S. Huck, *Nano Lett.*, 2008, **8**, 3819-3824.
10. M. Patra and P. Linse, *Nano Lett.*, 2006, **6**, 133-137.
11. W. K. Lee, M. Patra, P. Linse and S. Zauscher, *Small*, 2007, **3**, 63-66.
12. A. G. Koutsioubas and A. G. Vanakaras, *Langmuir*, 2008, **24**, 13717-13722.
13. A. M. Jonas, Z. Hu, K. Glinel and W. T. S. Huck, *Macromolecules*, 2008, **41**, 6859-6863.
14. M. Patra and P. Linse, *Macromolecules*, 2006, **39**, 4540-4546.
15. B. Zdyrko and I. Luzinov, *Macromol. Rapid Commun.*, 2011, **32**, 859-869.
16. R. Barbey, L. Lavanant, D. Paripovic, N. Schüwer, C. Sugnaux, S. Tugulu and H. A. Klok, *Chem. Rev.*, 2009, **109**, 5437-5527.
17. F. J. Xu, K. G. Neoh and E. T. Kang, *Prog. Polym. Sci.*, 2009, **34**, 719-761.
18. C. J. Fristrup, K. Jankova and S. Hvilsted, *Soft Matter*, 2009, **5**, 4623-4634.
19. F. Xia, Y. Zhu, L. Feng and L. Jiang, *Soft Matter*, 2009, **5**, 275-281.
20. Y. Tian, B. Su and L. Jiang, *Adv. Mater.*, 2014, **26**, 6872-6897.
21. K. Lee, S. Park, C. A. Mirkin, J. C. Smith and M. Mrksich, *Science*, 2002, **295**, 1702-1705.
22. B. K. Lee, H. Y. Lee, P. Kim, K. Y. Suh, J. H. Seo, H. J. Cha and T. Kawai, *Small*, 2008, **4**, 342-348.
23. E. K. Yim and K. W. Leong, *Nanomedicine*, 2005, **1**, 10-21.
24. P. Koeqler, A. Clayton, H. Thissen, G. N. Santos and P. Kingshott, *Adv. Drug Deliv. Rev.*, 2012, **64**, 1820-1839.
25. Q. Yu, L. M. Johnson and G. P. Lopez, *Adv. Funct. Mater.*, 2014, **24**, 3751-3759.
26. Q. Yu, J. Cho, P. Shivapooja, L. K. Ista and G. P. Lopez, *ACS Appl. Mater. Interfaces*, 2013, **5**, 9295-9304.
27. Q. Yu, L. K. Ista and G. P. Lopez, *Nanoscale*, 2014, **6**, 4750-4757.
28. L. K. Ista, Q. Yu, A. Parthasarathy, K. S. Schanze and G. P. Lopez, Unpublished data.
29. Q. Fu, G. V. Rama Rao, L. K. Ista, Y. Wu, B. Andrzejewski, L. A. Sklar, T. L. Ward and G. P. Lopez, *Adv. Mater.*, 2003, **15**, 1262-1266.
30. R. B. Vasani, S. J. P. McInnes, M. A. Cole, A. M. M. Jani, A. V. Ellis and N. H. Voelcker, *Langmuir*, 2011, **27**, 7843-7853.
31. Q. Yu, H. Chen, Y. Zhang, L. Yuan, T. Zhao, X. Li and H. Wang, *Langmuir*, 2010, **26**, 17812-17815.
32. Q. Fu, G. V. Rama Rao, S. B. Basame, D. J. Keller, K. Artyushkova, J. E. Fulghum and G. P. Lopez, *J. Am. Chem. Soc.*, 2004, **126**, 8904-8905.
33. G. Jeon, S. Y. Yang, J. Byun and J. K. Kim, *Nano Lett.*, 2011, **11**, 1284-1288.
34. P. De Gennes, *Adv. Colloid Interface Sci.*, 1987, **27**, 189-209.
35. S. Milner, T. Witten and M. Cates, *Macromolecules*, 1988, **21**, 2610-2619.
36. S. J. Ahn, M. Kaholek, W.-K. Lee, B. LaMattina, T. H. LaBean and S. Zauscher, *Adv. Mater.*, 2004, **16**, 2141-2145.
37. M. Steenackers, A. Kuller, N. Ballav, M. Zharnikov, M. Grunze and R. Jordan, *Small*, 2007, **3**, 1764-1773.

38. S. Kramer, R. R. Fuierer and C. B. Gorman, *Chem. Rev.*, 2003, **103**, 4367-4418.
39. Z. Xie, X. Zhou, X. Tao and Z. Zheng, *Macromol. Rapid Commun.*, 2012, **33**, 359-373.
40. J. H. Lim and C. A. Mirkin, *Adv. Mater.*, 2002, **14**, 1474-1477.
41. L. Li, M. Hirtz, W. Wang, C. Du, H. Fuchs and L. Chi, *Adv. Mater.*, 2010, **22**, 1374-1378.
42. R. Ferris, A. Hucknall, B. S. Kwon, T. Chen, A. Chilkoti and S. Zauscher, *Small*, 2011, **7**, 3032-3037.
43. R. D. Piner, *Science*, 1999, **283**, 661-663.
44. S. Hong, J. Zhu and C. A. Mirkin, *Science*, 1999, **286**, 523-525.
45. C. C. Wu, D. N. Reinhoudt, C. Otto, V. Subramaniam and A. H. Velders, *Small*, 2011, **7**, 989-1002.
46. B. W. Maynor, S. F. Filocamo, M. W. Grinstaff and J. Liu, *J. Am. Chem. Soc.*, 2001, **124**, 522-523.
47. R. McKendry, W. T. S. Huck, B. Weeks, M. Fiorini, C. Abell and T. Rayment, *Nano Lett.*, 2002, **2**, 713-716.
48. W. K. Lee, L. J. Whitman, J. Lee, W. P. King and P. E. Sheehan, *Soft Matter*, 2008, **4**, 1844-1847.
49. M. Hirtz, M. K. Brinks, S. Miele, A. Studer, H. Fuchs and L. Chi, *Small*, 2009, **5**, 919-923.
50. H. Wagner, Y. Li, M. Hirtz, L. Chi, H. Fuchs and A. Studer, *Soft Matter*, 2011, **7**, 9854-9858.
51. A. Rastogi, M. Y. Paik, M. Tanaka and C. K. Ober, *ACS Nano*, 2010, **4**, 771-780.
52. M. Y. Paik, Y. Xu, A. Rastogi, M. Tanaka, Y. Yi and C. K. Ober, *Nano Lett.*, 2010, **10**, 3873-3879.
53. E. ul-Haq, Z. M. Liu, Y. Zhang, S. A. A. Ahmad, L. S. Wong, J. K. Hobbs, G. J. Leggett, J. Micklefield, C. J. Roberts and J. M. R. Weaver, *J. Mater. Res.*, 2011, **26**, 2997-3008.
54. G. J. Leggett, *Chem. Soc. Rev.*, 2006, **35**, 1150-1161.
55. C. R. Hurley, R. E. Ducker, G. J. Leggett and B. D. Ratner, *Langmuir*, 2010, **26**, 10203-10209.
56. S. Alang Ahmad, A. Hucknall, A. Chilkoti and G. J. Leggett, *Langmuir*, 2010, **26**, 9937-9942.
57. N. Lomadze, A. Kopyshv, J. R  he and S. Santer, *Macromolecules*, 2011, **44**, 7372-7377.
58. A. Kopyshv, C. J. Galvin, J. Genzer, N. Lomadze and S. Santer, *Langmuir*, 2013, **29**, 13967-13974.
59. S. Edmondson, V. L. Osborne and W. T. S. Huck, *Chem. Soc. Rev.*, 2004, **33**, 14-22.
60. A. Mizutani, A. Kikuchi, M. Yamato, H. Kanazawa and T. Okano, *Biomaterials*, 2008, **29**, 2073-2081.
61. X. Jiang, H. Y. Chen, G. Galvan, M. Yoshida and J. Lahann, *Adv. Funct. Mater.*, 2008, **18**, 27-35.
62. S. Edmondson, C.-D. Vo, S. P. Armes, G.-F. Unali and M. P. Weir, *Langmuir*, 2008, **24**, 7208-7215.
63. X. Y. Chen, S. P. Armes, S. J. Greaves and J. F. Watts, *Langmuir*, 2004, **20**, 587-595.
64. P. Murugan, M. Krishnamurthy, S. N. Jaisankar, D. Samanta and A. B. Mandal, *Chem. Soc. Rev.*, 2015, **44**, 3212-3243.
65. B. Li, B. Yu, Q. Ye and F. Zhou, *Acc. Chem. Res.*, 2015, **48**, 229-237.
66. M. Krishnamoorthy, S. Hakobyan, M. Ramstedt and J. E. Gautrot, *Chem. Rev.*, 2014, **114**, 10976-11026.
67. A. Khabibullin, E. Mastan, K. Matyjaszewski and S. Zhu, *Adv. Polym. Sci.*, 2015, **270**, 29-76.
68. K. Matyjaszewski, *Macromolecules*, 2012, **45**, 4015-4039.
69. Y. Shen, H. Tang and S. Ding, *Prog. Polym. Sci.*, 2004, **29**, 1053-1078.
70. K. Matyjaszewski, H. Dong, W. Jakubowski, J. Pietrasik and A. Kusumo, *Langmuir*, 2007, **23**, 4528-4531.
71. K. Min, H. Gao and K. Matyjaszewski, *Macromolecules*, 2007, **40**, 1789-1791.
72. Y. Kwak, A. J. D. Magenau and K. Matyjaszewski, *Macromolecules*, 2011, **44**, 811-819.
73. P. Shivapooja, L. K. Ista, H. E. Canavan and G. P. Lopez, *Biointerphases*, 2012, **7**, 32.
74. B. T. Cheesman, J. D. Willott, G. B. Webber, S. Edmondson and E. J. Wanless, *ACS Macro Lett.*, 2012, **1**, 1161-1165.
75. S. Hansson, E. Ostmark, A. Carlmark and E. Malmstrom, *ACS Appl. Mater. Interfaces*, 2009, **1**, 2651-2659.
76. Y. Tsujii, M. Ejaz, K. Sato, A. Goto and T. Fukuda, *Macromolecules*, 2001, **34**, 8872-8878.
77. S. B. Rahane, J. A. Floyd, A. T. Metters and S. M. Kilbey, II, *Adv. Funct. Mater.*, 2008, **18**, 1232-1240.

78. R. Matsuno, K. Yamamoto, H. Otsuka and A. Takahara, *Macromolecules*, 2004, **37**, 2203-2209.
79. N. Y. Kim, N. L. Jeon, I. S. Choi, S. Takami, Y. Harada, K. R. Finnie, G. S. Girolami, R. G. Nuzzo, G. M. Whitesides and P. E. Laibinis, *Macromolecules*, 2000, **33**, 2793-2795.
80. Q. Y. Zhou, S. X. Wang, X. W. Fan, R. Advincula and J. Mays, *Langmuir*, 2002, **18**, 3324-3331.
81. R. Jordan and A. Ulman, *J. Am. Chem. Soc.*, 1998, **120**, 243-247.
82. B. Yameen and A. Farrukh, *Chem. Asian J.*, 2013, **8**, 1736-1753.
83. W. J. Brittain and S. Minko, *J. Polym. Sci., Part A: Polym. Chem.*, 2007, **45**, 3505-3512.
84. S. Edmondson and S. P. Armes, *Polym. Int.*, 2009, **58**, 307-316.
85. X. Liu, S. Guo and C. A. Mirkin, *Angew. Chem. Int. Ed.*, 2003, **42**, 4785-4789.
86. H. W. Ma, J. H. Hyun, P. Stiller and A. Chilkoti, *Adv. Mater.*, 2004, **16**, 338-341.
87. S. Zapotoczny, E. M. Benetti and G. J. Vancso, *J. Mater. Chem.*, 2007, **17**, 3293-3296.
88. M. Kaholek, W.-K. Lee, S.-J. Ahn, H. Ma, K. C. Caster, B. LaMattina and S. Zauscher, *Chem. Mater.*, 2004, **16**, 3688-3696.
89. M. Kaholek, W. K. Lee, B. LaMattina, K. C. Caster and S. Zauscher, *Nano Lett.*, 2004, **4**, 373-376.
90. X. Liu, Y. Li and Z. Zheng, *Nanoscale*, 2010, **2**, 2614-2618.
91. X. C. Zhou, X. L. Wang, Y. D. Shen, Z. Xie and Z. J. Zheng, *Angew. Chem. Int. Ed.*, 2011, **50**, 6506-6510.
92. X. Zhou, Z. Liu, Z. Xie, X. Liu and Z. Zheng, *Small*, 2012, **8**, 3568-3572.
93. W. K. Lee, K. C. Caster, J. Kim and S. Zauscher, *Small*, 2006, **2**, 848-853.
94. E. M. Benetti, H. J. Chung and G. J. Vancso, *Macromol. Rapid Commun.*, 2009, **30**, 411-417.
95. Y. Tsujii, M. Ejaz, S. Yamamoto, T. Fukuda, K. Shigeto, K. Mibu and T. Shinjo, *Polymer*, 2002, **43**, 3837-3841.
96. M. Kaholek, W. K. Lee, J. X. Feng, B. LaMattina, D. J. Dyer and S. Zauscher, *Chem. Mater.*, 2006, **18**, 3660-3664.
97. A. M. Jonas, K. Glinel, R. Oren, B. Nysten and W. T. S. Huck, *Macromolecules*, 2007, **40**, 4403-4405.
98. A. Pallandre, K. Glinel, A. M. Jonas and B. Nysten, *Nano Lett.*, 2004, **4**, 365-371.
99. Ursula Schmelmer, Rainer Jordan, Wolfgang Geyer, Wolfgang Eck, Armin Golzhauser, Michael Grunze and Abraham Ulman, *Angew. Chem. Int. Ed.*, 2003, **42**, 559-563.
100. U. Schmelmer, A. Paul, A. Kuller, M. Steenackers, A. Ulman, M. Grunze, A. Golzhauser and R. Jordan, *Small*, 2007, **3**, 459-465.
101. Q. He, A. Küller, M. Grunze and Junbai Li, *Langmuir*, 2007, **23**, 3981-3987.
102. Q. He, A. Kueller, S. Schilp, F. Leisten, H.-A. Kolb, M. Grunze and J. Li, *Small*, 2007, **3**, 1860-1865.
103. N. Ballav, S. Schilp and M. Zharnikov, *Angew. Chem.*, 2008, **120**, 1443-1446.
104. M. Steenackers, R. Jordan, A. Küller and M. Grunze, *Adv. Mater.*, 2009, **21**, 2921-2925.
105. M. Steenackers, I. D. Sharp, K. Larsson, N. A. Hutter, M. Stutzmann and R. Jordan, *Chem. Mater.*, 2010, **22**, 272-278.
106. N. A. Hutter, M. Steenackers, A. Reitingner, O. A. Williams, J. A. Garrido and R. Jordan, *Soft Matter*, 2011, **7**, 4861-4867.
107. I. Amin, M. Steenackers, N. Zhang, R. Schubel, A. Beyer, A. Golzhauser and R. Jordan, *Small*, 2011, **7**, 683-687.
108. D. Xia, Z. Ku, S. C. Lee and S. R. Brueck, *Adv. Mater.*, 2011, **23**, 147-179.
109. G. Tizazu, O. El-Zubir, S. R. Brueck, D. G. Lidzey, G. J. Leggett and G. P. Lopez, *Nanoscale*, 2011, **3**, 2511-2516.
110. G. Tizazu, O. El-Zubir, S. Patole, A. McLaren, C. Vasilev, D. J. Mothersole, A. Adawi, C. N. Hunter, D. G. Lidzey, G. P. Lopez and G. J. Leggett, *Biointerphases*, 2012, **7**, 54.
111. C. Schuh, S. Santer, O. Prucker and J. Ruhe, *Adv. Mater.*, 2009, **21**, 4706-4710.
112. S. A. Ahmad, G. J. Leggett, A. Hucknall and A. Chilkoti, *Biointerphases*, 2011, **6**, 8-15.
113. S. R. J. Brueck, *P. IEEE*, 2005, **93**, 1704-1721.

114. C. Padeste, P. Farquet, C. Potzner and H. H. Solak, *J. Biomater. Sci., Polym. Ed.*, 2006, **17**, 1285-1300.
115. S. Neuhaus, C. Padeste, H. H. Solak and N. D. Spencer, *Polymer*, 2010, **51**, 4037-4043.
116. H.-P. Brack, C. Padeste, M. Slaski, S. Alkan and H. H. Solak, *J. Am. Chem. Soc.*, 2004, **126**, 1004-1005.
117. Y. Ofir, I. W. Moran, C. Subramani, K. R. Carter and V. M. Rotello, *Adv. Mater.*, 2010, **22**, 3608-3614.
118. S. B. Jhaveri, M. Beinhoff, C. J. Hawker, K. R. Carter and D. Y. Sogah, *ACS Nano*, 2008, **2**, 719-727.
119. Matthias Beinhoff, Anjuli T. Appapillai, Leah D. Underwood, Jane E. Frommer and K. R. Carter, *Langmuir*, 2006, **22**, 2411-2414.
120. Timothy A. von Werne, David S. Germack, Erik C. Hagberg, Valerie V. Sheares, Craig J. Hawker and K. R. Carter, *J. Am. Chem. Soc.*, 2003, **125**, 3831 -3838.
121. K. Y. Suh, Y. S. Kim and H. H. Lee, *Adv. Mater.*, 2001, **13**, 1386-1389.
122. K. Y. Suh and H. H. Lee, *Adv. Funct. Mater.*, 2002, **12**, 405-413.
123. Y. Liu, V. Klep and I. Luzinov, *J. Am. Chem. Soc.*, 2006, **128**, 8106-8107.
124. B. Gupta, Y. Zhu, B. Guan, P. J. Reece and J. J. Gooding, *Analyst*, 2013, **138**, 3593-3615.
125. Q. Yu, H. Liu and H. Chen, *J. Mater. Chem. B*, 2014, **2**, 7849-7860.
126. A. M. Md Jani, D. Losic and N. H. Voelcker, *Prog. Mater. Sci.*, 2013, **58**, 636-704.
127. K. Huo, B. Gao, J. Fu, L. Zhao and P. K. Chu, *RSC Adv.*, 2014, **4**, 17300-17324.
128. W. Kim, J. K. Ng, M. E. Kunitake, B. R. Conklin and P. D. Yang, *J. Am. Chem. Soc.*, 2007, **129**, 7228-7229.
129. B. S. Kim, S. Shin, S. J. Shin, K. M. Kim and H. H. Cho, *Langmuir*, 2011, **27**, 10148-10156.
130. M. L. Bruening, D. M. Dotzauer, P. Jain, L. Ouyang and G. L. Baker, *Langmuir*, 2008, **24**, 7663-7673.
131. L. Britcher, T. J. Barnes, H. J. Griesser and C. A. Prestidge, *Langmuir*, 2008, **24**, 7625-7627.
132. Q. Yu, X. Li, Y. Zhang, L. Yuan, T. Zhao and H. Chen, *RSC Adv.*, 2011, **1**, 262-269.
133. K. Liu, X. Yao and L. Jiang, *Chem. Soc. Rev.*, 2010, **39**, 3240-3255.
134. M. Liu, Y. Zheng, J. Zhai and L. Jiang, *Acc. Chem. Res.*, 2010, **43**, 368-377.
135. X. Yao, Y. Song and L. Jiang, *Adv. Mater.*, 2011, **23**, 719-734.
136. J. Drelich, E. Chibowski, D. D. Meng and K. Terpilowski, *Soft Matter*, 2011, **7**, 9804-9828.
137. Y. Y. Yan, N. Gao and W. Barthlott, *Adv. Colloid Interface Sci.*, 2011, **169**, 80-105.
138. D. Qurere, *Annu. Rev. Mater. Res.*, 2008, **38**, 71-99.
139. F. Xia and L. Jiang, *Adv. Mater.*, 2008, **20**, 2842-2858.
140. R. N. Wenzel, *Ind. Eng. Chem.*, 1936, **28**, 988-994.
141. A. B. D. Cassie and S. Baxter, *Trans. Faraday Soc.*, 1944, **40**, 546-551.
142. G. Piret, Y. Coffinier, C. Roux, O. Melnyk and R. Boukherroub, *Langmuir*, 2008, **24**, 1670-1672.
143. K. Liu and L. Jiang, *Nanoscale*, 2011, **3**, 825-838.
144. J. Wang, Y. Zhang, S. Wang, Y. Song and L. Jiang, *Acc. Chem. Res.*, 2011, **44**, 405-415.
145. M. A. Cole, N. H. Voelcker, H. Thissen and H. J. Griesser, *Biomaterials*, 2009, **30**, 1827-1850.
146. P. M. Mendes, *Chem. Soc. Rev.*, 2008, **37**, 2512-2529.
147. T. L. Sun, G. J. Wang, L. Feng, B. Q. Liu, Y. M. Ma, L. Jiang and D. B. Zhu, *Angew. Chem. Int. Ed.*, 2004, **43**, 357-360.
148. F. Xia, L. Feng, S. T. Wang, T. L. Sun, W. L. Song, W. H. Jiang and L. Jiang, *Adv. Mater.*, 2006, **18**, 432-436.
149. F. Xia, H. Ge, Y. Hou, T. L. Sun, L. Chen, G. Z. Zhang and L. Jiang, *Adv. Mater.*, 2007, **19**, 2520-2524.
150. L. Wang, H. Wang, L. Yuan, W. Yang, Z. Wu and H. Chen, *J. Mater. Chem.*, 2011, **21**, 13920-13925.
151. C. J. Wilson, R. E. Clegg, D. I. Leavesley and M. J. Percy, *Tissue Eng.*, 2005, **11**, 1-18.
152. A. L. Hook, H. Thissen and N. H. Voelcker, *Trends Biotechnol.*, 2006, **24**, 471-477.
153. P. Jonkheijm, D. Weinrich, H. Schroder, C. M. Niemeyer and H. Waldmann, *Angew. Chem. Int. Ed.*, 2008, **47**,

- 9618-9647.
154. P. C. Lin, D. Weinrich and H. Waldmann, *Macromol. Chem. Phys.*, 2010, **211**, 136-144.
 155. K. L. Christman, V. D. Enriquez-Rios and H. D. Maynard, *Soft Matter*, 2006, **2**, 928-939.
 156. P. M. Mendes, C. L. Yeung and J. A. Preece, *Nanoscale Res. Lett.*, 2007, **2**, 373-384.
 157. R. Ogaki, M. Alexander and P. Kingshott, *Mater. Today*, 2010, **13**, 22-35.
 158. S. Jiang and Z. Cao, *Adv. Mater.*, 2010, **22**, 920-932.
 159. Q. Yu, Y. Zhang, H. Wang, J. L. Brash and H. Chen, *Acta Biomater.*, 2011, **7**, 1550-1557.
 160. H. Jiang and F. J. Xu, *Chem. Soc. Rev.*, 2013, **42**, 3394-3426.
 161. I. Banerjee, R. C. Pangule and R. S. Kane, *Adv. Mater.*, 2011, **23**, 690-718.
 162. Y. Hong, P. Krsko and M. Libera, *Langmuir*, 2004, **20**, 11123-11126.
 163. D. Falconnet, D. Pasqui, S. Park, R. Eckert, H. Schiff, J. Gobrecht, R. Barbucci and M. Textor, *Nano Lett.*, 2004, **4**, 1909-1914.
 164. J. Y. Lim and H. J. Donahue, *Tissue Eng.*, 2007, **13**, 1879-1891.
 165. E. Martinez, E. Engel, C. Lopez-Iglesias, C. A. Mills, J. A. Planell and J. Samitier, *Micron*, 2008, **39**, 111-116.
 166. A. M. Ross, Z. Jiang, M. Bastmeyer and J. Lahann, *Small*, 2012, **8**, 336-355.
 167. K. Kulangara and K. W. Leong, *Soft Matter*, 2009, **5**, 4072-4076.
 168. X. Liu and S. Wang, *Chem. Soc. Rev.*, 2014, **43**, 2385-2401.
 169. P. M. Mendes, *Chem. Soc. Rev.*, 2013, **42**, 9207-9218.
 170. X. Lin, Q. He and J. Li, *Chem. Soc. Rev.*, 2012, **41**, 3584-3593.
 171. J. Genzer and R. R. Bhat, *Langmuir*, 2008, **24**, 2294-2317.
 172. R. R. Bhat, M. R. Tomlinson, T. Wu and J. Genzer, *Adv. Polym. Sci.*, 2006, **198**, 51-124.
 173. R. R. Bhat, B. N. Chaney, J. Rowley, A. Liebmann-Vinson and J. Genzer, *Adv. Mater.*, 2005, **17**, 2802-2807.
 174. L. Li, Y. Zhu, B. Li and C. Gao, *Langmuir*, 2008, **24**, 13632-13639.
 175. M. S. Kim, G. Khang and H. B. Lee, *Prog. Polym. Sci.*, 2008, **33**, 138-164.
 176. D. Roy, J. N. Cambre and B. S. Sumerlin, *Prog. Polym. Sci.*, 2010, **35**, 278-301.
 177. M. A. C. Stuart, W. T. S. Huck, J. Genzer, M. Muller, C. Ober, M. Stamm, G. B. Sukhorukov, I. Szleifer, V. V. Tsukruk, M. Urban, F. Winnik, S. Zauscher, I. Luzinov and S. Minko, *Nat. Mater.*, 2010, **9**, 101-113.
 178. H. G. Schild, *Prog. Polym. Sci.*, 1992, **17**, 163-249.
 179. J. Kim, J. Yoon and R. C. Hayward, *Nat. Mater.*, 2010, **9**, 159-164.
 180. C. D. H. Alarcon, T. Farhan, V. L. Osborne, W. T. S. Huck and C. Alexander, *J. Mater. Chem.*, 2005, **15**, 2089-2094.
 181. H. Takahashi, M. Nakayama, K. Itoga, M. Yamato and T. Okano, *Biomacromolecules*, 2011, **12**, 1414-1418.
 182. T. Chen, D. P. Chang, J. Zhang, R. Jordan and S. Zauscher, *Adv. Funct. Mater.*, 2012, **22**, 429-434.
 183. H. Tu, C. E. Heitzman and P. V. Braun, *Langmuir*, 2004, **20**, 8313-8320.
 184. X. Wang, H. Tu, P. V. Braun and P. W. Bohn, *Langmuir*, 2006, **22**, 817-823.
 185. Q. Yu, Y. Zhang, H. Chen, Z. Wu, H. Huang and C. Cheng, *Colloids Surf., B*, 2010, **76**, 468-474.
 186. L. K. Ista, S. Mendez, S. S. Balamurugan, S. Balamurugan, V. G. Rama Rao and G. P. Lopez, *ACS Symp. Ser.*, 2009, **1002**, 95-110.
 187. L. K. Ista, S. Mendez and G. P. Lopez, *Biofouling*, 2010, **26**, 111-118.
 188. L. K. Ista, V. H. Perez-Luna and G. P. Lopez, *Appl. Environ. Microbiol.*, 1999, **65**, 1603-1609.
 189. D. Cunliffe, C. D. Alarcon, V. Peters, J. R. Smith and C. Alexander, *Langmuir*, 2003, **19**, 2888-2899.
 190. Q. Yu, W. Ge, A. Atewologun, A. D. Stiff-Roberts and G. P. López, *Colloids Surf., B*, 2015, **126**, 328-334.
 191. Q. Yu, W. Ge, A. Atewologun, A. D. Stiff-Roberts and G. P. Lopez, *J. Mater. Chem. B*, 2014, **2**, 4371-4378.
 192. Q. Yu, Z. Wu and H. Chen, *Acta Biomater.*, 2015, **16**, 1-13.

193. M. Yamato, Y. Akiyama, J. Kobayashi, J. Yang, A. Kikuchi and T. Okano, *Prog. Polym. Sci.*, 2007, **32**, 1123-1133.
194. M. A. Cooperstein and H. E. Canavan, *Langmuir*, 2010, **26**, 7695-7707.
195. P. Li, R. Xie, J. Jiang, T. Meng, M. Yang, X.-J. Ju, L. Yang and L. Chu, *J. Membr. Sci.*, 2009, **337**, 310-317.
196. Z. Y. Zhou, S. M. Zhu and D. Zhang, *J. Mater. Chem.*, 2007, **17**, 2428-2433.
197. R. Liu, P. Liao, J. Liu and P. Feng, *Langmuir*, 2011, **27**, 3095-3099.
198. X. Hou, F. Yang, L. Li, Y. Song, L. Jiang and D. Zhu, *J. Am. Chem. Soc.*, 2010, **132**, 11736-11742.
199. J. Xue, L. Chen, H. L. Wang, Z. B. Zhang, X. L. Zhu, E. T. Kang and K. G. Neoh, *Langmuir*, 2008, **24**, 14151-14158.
200. R. R. Shah, D. Merreceyes, M. Husemann, I. Rees, N. L. Abbott, C. J. Hawker and J. L. Hedrick, *Macromolecules*, 2000, **33**, 597-605.
201. W. T. S. Huck, L. Yan, A. Stroock, R. Haag and G. M. Whitesides, *Langmuir*, 1999, **15**, 6862-6867.
202. D. Mijatovic, J. C. T. Eijkel and A. van den Berg, *Lab on a chip*, 2005, **5**, 492-500.
203. W. T. S. Huck, *Mater. Today*, 2008, **11**, 24-32.
204. K. Sathiyaraj, M. Harshiny, B. Nazeema Banu, K. Rajendran and S. Kumaran, *Superlattice Microst*, 2011, **49**, 581-590.